

### **Abstract**

This is a collection of documents describing a design and performance of an off-axis detector utilizing glass RPC. It is intended to serve as a base for writing a proposal for the experiment after necessary edits, corrections, additions and deletions.

# Contents

<b>1</b>	<b>Detector</b>	<b>3</b>
1.1	Overview	3
1.1.1	Detector geometry	4
1.1.2	Module geometry	6
1.1.3	Absorber planes	8
1.1.4	Detector unit	8
1.1.5	RPC chambers	9
1.1.6	Readout boards	10
1.1.7	Detector unit assembly	10
1.2	Glass RPC Chambers	10
1.2.1	Principle of operation	10
1.2.2	The design of the Off-axis detector RPC's	12
1.2.3	The performance of RPC's	12
1.2.4	Construction of Resistive Plate Chambers (RPCs)	15
1.3	Signal Readout	17
1.3.1	RPC signals	17
1.3.2	RPC readout boards	18
1.3.3	Signal Collection	20
1.4	High Voltage Supply and Control	21
1.4.1	Overview	21
1.4.2	High Voltage Generation	22
1.4.3	System Control	23
1.4.4	Power	24
1.5	Readout Electronics	24
1.5.1	Overview	24
1.5.2	Front End ASIC	26
1.5.3	Data Concentrator	26
1.5.4	Data Collector	26
1.5.5	VME Crate	27
1.5.6	Physical Configuration on Detector	27
1.6	Absorber/RPC unit design and construction	34
1.6.1	Overview	34
1.6.2	Components	34
1.6.2.1	Readout boards	35

1.6.2.2	Absorber boards . . . . .	35
1.6.3	RRA Assembly . . . . .	35
1.6.4	Horizontal readout board units . . . . .	36
1.6.5	Vertical readout boards . . . . .	36
1.6.6	RPC Layers on HRU . . . . .	36
1.6.7	HV, signal and gass connections . . . . .	37
1.7	Detector construction . . . . .	37
1.8	Design of a Gas System . . . . .	39
1.8.1	General Description . . . . .	39
1.8.2	Gas specification and cost . . . . .	39
1.8.3	Gas flammability . . . . .	41
1.8.4	Glass thickness and spacer pitch . . . . .	41
1.8.5	Barometric Pressure . . . . .	41
1.8.6	Gas Distribution System . . . . .	41
1.8.7	Gas Storage . . . . .	42
1.8.8	Circulation . . . . .	42
1.8.9	Mixing . . . . .	43
1.8.10	Materials . . . . .	43
1.8.11	Pressure Relief . . . . .	43
1.8.12	Gas Analysis . . . . .	44
1.8.13	Instrumentation . . . . .	44
1.8.14	Controls and Alarms . . . . .	44
1.8.15	Procedures . . . . .	45
1.8.16	Prototype . . . . .	45
1.8.17	What-if Analysis . . . . .	45
1.9	Cosmic Rays Background and a Veto Shield . . . . .	46
1.10	Near Detector . . . . .	46
1.11	ES&H . . . . .	48
1.11.1	Fire . . . . .	48
1.11.2	Lifting heavy loads . . . . .	49
1.11.3	Glass handling hazards . . . . .	49
1.11.4	Oxygen Deficiency Hazard . . . . .	49
1.11.5	Fall Protection . . . . .	49
1.12	Operation and Maintenance . . . . .	49
1.13	Installation of the detector . . . . .	50
1.14	Detector Enclosure, Infrastructure, Access to Detector . . . . .	51
<b>2</b>	<b>Analysis and Physics capabilities</b>	<b>55</b>
2.1	The generated event sample . . . . .	55
2.2	The beam spectra and oscillation parameters used . . . . .	56
2.3	The reconstruction of events . . . . .	57
2.4	The overall background rejection strategy . . . . .	58
2.4.1	The loose cuts . . . . .	59
2.4.2	The likelihood functions . . . . .	60
2.5	Results . . . . .	61
2.6	The sensitivity as a function of absorber thickness . . . . .	64

2.7	The sensitivity as a function of active plane positions . . . . .	64
2.8	Differences between $\nu_\mu \rightarrow \nu_e$ and $\bar{\nu}_\mu \rightarrow \bar{\nu}_e$ . . . . .	66
2.9	Strip width studies . . . . .	68
2.10	Chamber efficiency studies . . . . .	68
2.11	Cross Talk studies . . . . .	69
2.12	Dead space studies . . . . .	71
2.13	Fiducial volume studies . . . . .	72
	References . . . . .	76

# Chapter 1

## Detector

### 1.1 Overview

To take full advantage of the physics opportunity provided by the NuMI beam it is necessary to construct a detector capable of detecting and identifying with high efficiency the  $\nu_e$  charged current interactions while, at the same time providing an adequate rejection power against the  $\nu_\mu$  neutral current and charged current background. The detector should be optimized for the neutrino energy range of  $1 - 3 \text{ GeV}$ .

Such a detector must meet several challenges:

- it must have fine granularity in order to identify the final state electrons
- it must have very large mass to provide maximal sensitivity to the oscillation amplitude
- it must have an acceptable cost per unit mass

A fine granularity low Z sampling calorimeter, following the examples of CHARM [1], FIMM [2] and CHARM II [3] experiments, is the natural detector choice. The low Z absorber maximizes the detector mass at the desired sampling frequency  $\Delta X_0$ , where  $X_0$  is the radiation length. We have adopted  $1/3 X_0$  sampling frequency for a baseline design.

A standard building material, particleboard, is a very convenient, commercially available, target material. It has very good mechanical properties and can be produced in  $8' \times 28'$  ( $2.43\text{m} \times 8.53 \text{ m}$ ) sheets  $2.54 \text{ cm}$  thick.

The low rate environment of a neutrino experiment makes it possible to utilize glass Resistive Plate Chambers (RPC) with strip readout, as active detectors. These detectors have an excellent track record (BELLE [4], HARP [5]), and have to be distinguished from some less successful implementations of bakelite RPC's.

RPC chambers are detectors of choice for large area, low-maintenance experiments in remote locations. Examples of uses or of proposed uses of very large areas of RPC chambers include

- AUGER experiment in Argentina [?]
- ARGO experiment in Tibet [7]
- Monolith experiment in Gran Sasso [8]
- Indian Neutrino Observatory in XXX [9]
- energy flow calorimeter [10] and muon detectors [11] for the Linear Collider experiment

Very attractive features of the glass RPC's include:

- two-dimensional positional information from every plane of detectors, thus maximizing the topological information about the neutrino event
- uniform response over the entire area of the detector
- very large induced signals (in a streamer mode), thus requiring simple and inexpensive electronics
- simplicity of construction leading to long term stability and low production costs [12]

Particles produced in low energy neutrino interactions are typically emitted at large angles,  $20 - 30^\circ$ . Their energies are often below the threshold for inelastic interactions, hence they will often range out in a low density detector. To maximize a fiducial mass it is therefore very important to construct a detector with large transverse dimensions of the order of  $15\text{ m}$  or more. The construction of a detector of such dimensions is a challenging proposition requiring very detailed engineering studies.

It is highly desirable that the detector is constructed in a modular fashion. This will facilitate the construction of the detector and enable distribution of the production effort over the collaborating institutions. More importantly, however, such a detector will allow, at least in principle, moving the detector to some other location, should the initial results indicate that such a move would enhance the physics capabilities of the experiment.

### 1.1.1 Detector geometry

The detector consists of 1200 modules each  $8.534\text{ m}$  long,  $2.438\text{ m}$  high and  $2.6\text{ m}$  deep. Modules are stacked in an array consisting of 75 planes along the beam direction, each plane being 2 modules wide and 8 high, as shown in Fig. 1.1. This provides a high degree of hermeticity: the gap at the center of the detector between two side by side modules is kept to  $5\text{ mm}$ . The distance between the modules along the beam axis is chosen to simplify the stacking and unstacking procedure and is of the order of  $5\text{ cm}$ . The overall dimensions of the detector are:  $17.1 \times 19.5 \times 233.2\text{ m}^3$ .

Walls of modules are supported from the floor and are not connected to each other. Modules within each wall are interlocked with the help of corner

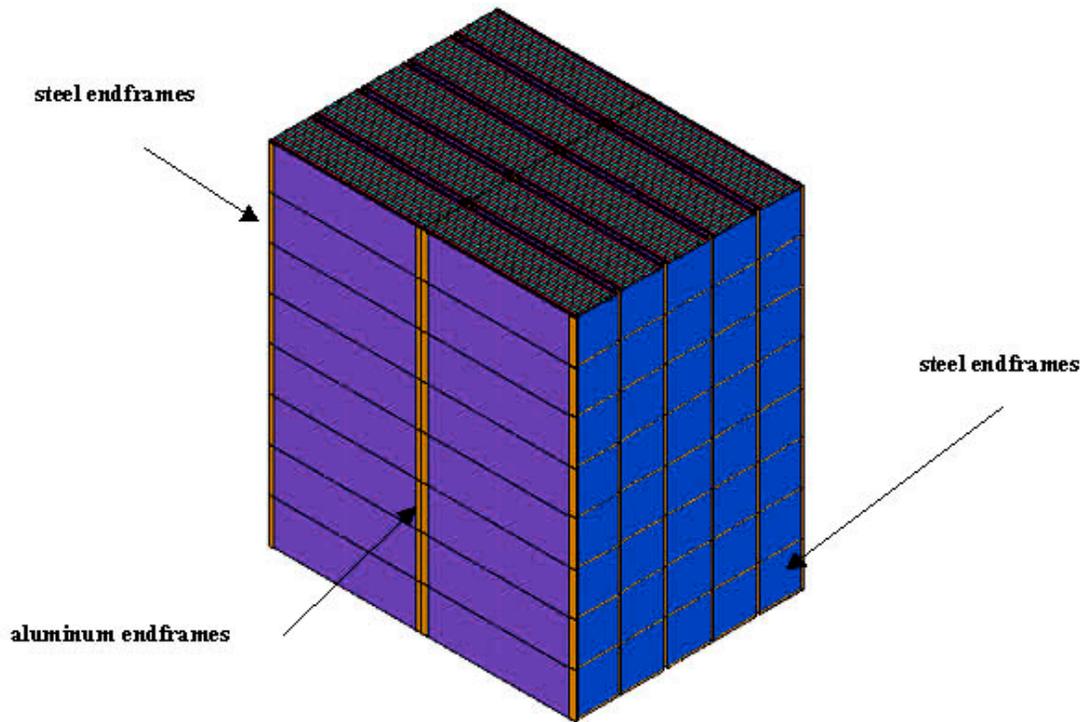


**Figure 2. Portion of Detector Module Array**

Figure 1.1: Five planes of the stacked modules.

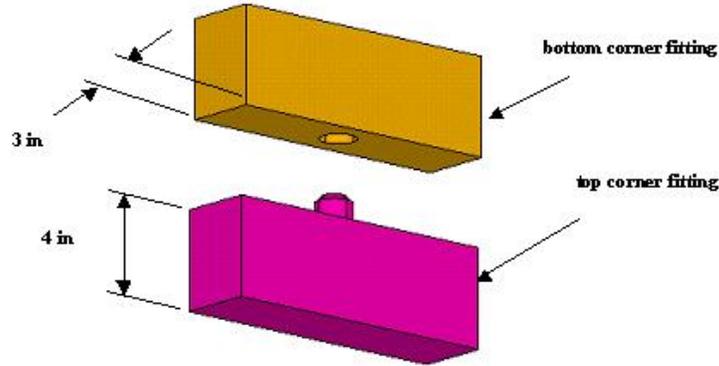


Figure 1.2: Module corner fittings. They are embedded in the top and bottom of the composite column.

blocks, Fig. 1.2, similar to those used in the standard shipping containers. Readout electronics and gas distribution and recirculation lines are mounted on both sides of the detector and are readily accessible during the operation of the experiment.

Experience with large systems of glass RPC's indicates that there is no need to replace or repair them. To minimize further a potential need for the replacement we have adopted a design providing redundancy by locating two independent planes of chambers at each active detector plane. Nonetheless, in the event of an unexpected large scale failure of the chambers, their replacement will be possible by unstacking the relevant modules, replacing the defective chambers and restacking the modules. It is worth noting that each vertical column of modules can be unstacked without affecting its neighbors.

### 1.1.2 Module geometry

Each module consists of 12 vertical planes of absorber interleaved with double planes of Resistive Plate Chambers. Two end-plates, Fig. 1.3 provide the mechanical rigidity of the module. In order to minimize the amount of dead material in the fiducial volume of the detector, the end plates located in the center of the detector are made of 0.3175cm thick aluminum. The other end plates, located at the edge of the detector, are constructed out of steel. The weight of the module is supported by two bottom angles, 1.27 cm thick and  $15.24 \times 15.24$  cm wide and subsequently transferred to four corner posts. These posts ultimately transfer the load to the floor in a manner analogous to the posts in a standard shipping container.

To minimize the dead material in the fiducial volume the corner posts are composed of two aluminium plates,  $1.27 \times 25.4 \times 243.8$  cm, sandwiched around

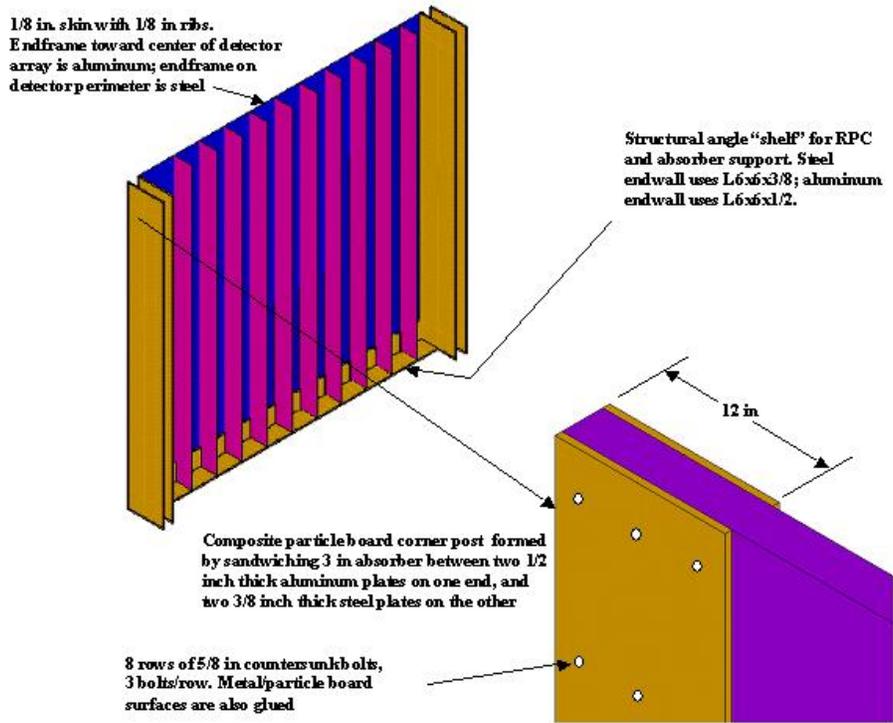


Figure 1.3: End plate and the corner post.

a 7.62 *cm* thick particle board. At the outer edge of the module the plates are made of steel, thus reducing the cost and reinforcing the structure at the same time. These posts are part of the absorber structure and represent only a small degradation of the sampling of the detector: an additional 0.25  $X_0$  over 6% of the area of only 6% of the absorber planes.

To support the load of the module the bottom angles are reinforced by welding ten ribs (aluminum at the center, steel at the periphery) 0.3175 *cm* thick and 15.24 *cm* wide. Absorber/RPC assemblies attached to the corner posts and to the ribs create a toaster-like structure, Fig.1.4.

Module frame, after the proper checkout of the detector elements, will be shipped to the experimental site where it will be filled with the remaining absorber planes, see Fig. 1.5.

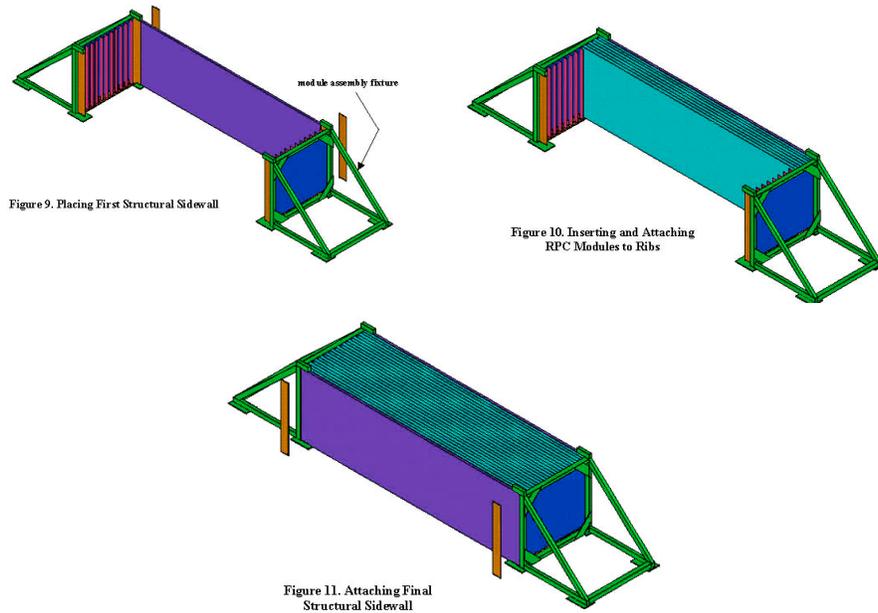


Figure 1.4: Construction of a toaster.

### 1.1.3 Absorber planes

There are 13 absorber planes in a module. The central eleven are 15.24cm thick and are assembled out of 6 boards 8.534m long, 2.438m wide and 2.54cm thick held together by glue and screws. The first and last absorber planes are constructed in a similar manner but are half as thick. Thus, when taken together with the first and last planes of preceding and succeeding modules, they result in a uniform sampling thickness across module boundaries. The absorber planes have 1.27 cm deep and 15.24 cm long notches at the bottom corners to accommodate the weight-supporting angles on which they rest. In addition each of the eleven central planes is attached to a vertical reinforcing rib mounted on each of the two end plates. The support for the other two planes is provided by the corner posts which are an integral part of them.

### 1.1.4 Detector unit

A detector unit consists of two planes of glass RPC's sandwiched between two particle boards, the readout boards, one carrying the horizontal readout strips and the other the vertical ones. The boards also serve as a protection for the glass chambers.

A detector unit is 8.534 m long and 2.438 m high. It also has 1.27 cm deep

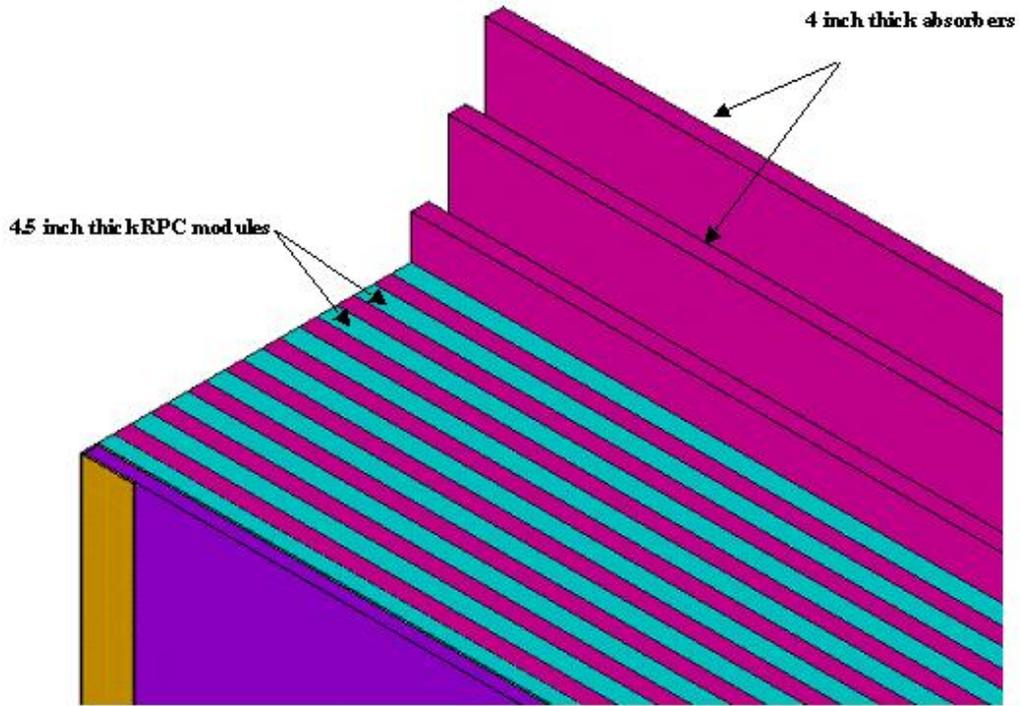


Figure 1.5: Insertion of the absorber planes into a "toaster".

and 15.24 *cm* long notches at the bottom corners to accommodate the weight-supporting angles on which they rest. Therefore the chambers only cover an area of  $8.509 \times 2.425 \text{ m}^2$  resulting in a dead space due to the support structure of the order of 0.4%.

### 1.1.5 RPC chambers

Chambers are constructed in a manner very similar to the BELLE chambers. The chambers are  $2.844 \times 2.425 \text{ m}^2$  large and are constructed from 3 *mm* thick float glass. A uniform distance between the glass plates, which defines the electric field in the chamber is ensured by 2 *mm* thick Noryl spacers, 15 *cm* apart, and glued to both glass plates. These spacers, glued in a maze-like pattern, serve several purposes:

- ensure a uniform gas flow over the entire area of the chamber
- define a uniform distance between the glass plates

- protect the chamber from breaking in the event of a sudden change of atmospheric pressure. With 3 *mm* glass and 15 *cm* between spacers chambers can withstand a difference between the internal and atmospheric pressures of up to 0.04 *atm*.

The outer perimeter of the glass plates is sealed with a T-shaped extruded Noryl border to provide a gas-tight volume.

The corners of the chambers are cut at a 45° angle. Triangular, injection molded, plastic pieces are glued in. They contain the gas inlet and outlet.

The outer surfaces of the glass are painted with a resistive paint. High voltage leads are soldered to a copper pad glued to these resistive layers. An insulating plastic sheet covers the entire surface of the chamber.

### 1.1.6 Readout boards

The two readout boards, each 8.534 *m* long and 2.438 *m* high, form the covers of the detector unit, with two planes of glass RPC's sandwiched between them. Both surfaces of both readout boards have thin copper foils glued to them. The copper foil on surfaces facing the chambers is cut into strips (horizontal on one board and vertical on the other) to provide the capacitive readout. The foil on the other surface is a ground plane thus resulting in a transmission line.

The horizontal strips are 3.7 *cm* wide with 3.8 *cm* pitch, whereas the vertical ones are 4.34 *cm* wide with 4.44 *cm* pitch. Each detector unit has, therefore 192 vertical readout strips and 64 horizontal ones.

### 1.1.7 Detector unit assembly

Three glass chambers are positioned on the first readout board to cover the entire active area. A second plane of glass chambers is positioned on top of the first one. The internal spacers of the chambers in the two layers are displaced with respect to each other to maximize the detection efficiency.

The second read out board is then positioned on top of the second RPC plane and secured to the first readout board by means of bolts traversing the assembly in the region of the triangular corner pieces. U-shaped clips at the bottom of the unit support the weight of the chambers.

Daisy-chained gas lines provide a common gas flow for the three chambers in a plane. A separate high voltage supply, including current readback, is provided for every chamber. Gas lines and high voltage lines are fed from the outer edge of the detector unit.

## 1.2 Glass RPC Chambers

### 1.2.1 Principle of operation

Glass RPC chambers belong to the family of Resistive Plate Chambers, but they utilize inexpensive commercial float glass of high resistivity ( $10^{12} \Omega\text{cm}$ )

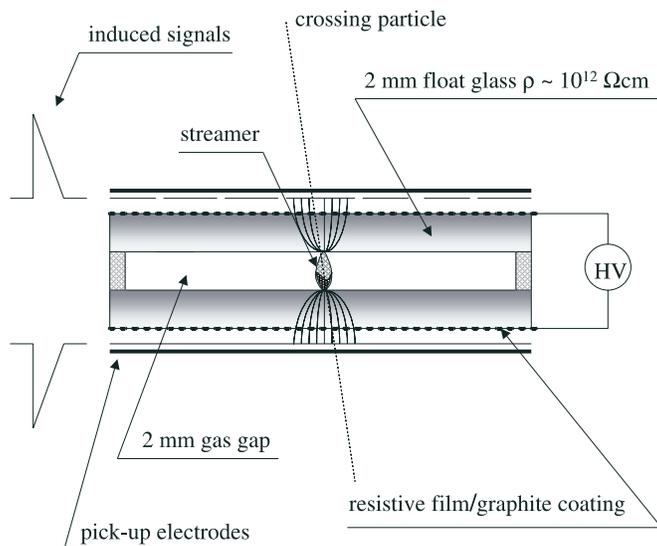


Figure 1.6: Glass RPC detector principle

instead of the traditional bakelite.

The detector, shown in Fig. 1.6, is composed of two parallel glass electrodes, 3 mm thick, kept 2 mm apart by appropriate spacers. The gap between electrodes is filled with a suitable non-flammable gas mixture. The resistive coating on the outer surfaces of the glass connected to the HV power supply creates a strong electric field  $\sim 4 \div 5 \text{ kV/mm}$  across the gap. An ionizing particle initiates a local discharge, a streamer, which induces a signal on external pickup electrodes, usually strips. The high resistivity of the glass and the quenching properties of the gas limit the discharge to a small area.

By locating pickup electrodes on both sides of the chamber and by making the orientation of the strips in the two electrodes orthogonal to each other, two coordinates can be obtained from a single RPC gap. Note that signals of opposite polarity are induced on the two electrodes. The pickup electrodes consist of a plane of metallic strips glued to an insulating layer on the other side of which is glued another metallic plane held at ground. This transforms the pickup strips into transmission lines, thus allowing the signals to be transported over long strip lengths. The induced pulses are typically 100–300 mV/50Ω with  $\sim \text{ns}$  time resolution. Large signals of 100–200 pC allow for the possibility of a variety of cost saving options in the readout electronics.

This type of detector does not have the rate capability necessary for hadron colliders but, is more than adequate for low rate applications such as this neutrino experiment. This has been demonstrated by the BELLE experiment at

KEK [4] which has successfully used them for muon and K-long detection.

They are ideal for large area applications since the pickup strips can be configured as transmission lines covering many meters in length. Furthermore they are relatively simple and inexpensive to construct. Their typical cost is in the range of  $\$100 - 150/m^2$  of the detector [12, ?]. As an example, the Monolith [8] group has developed a design for RPC planes as large as  $15 \times 30 m^2$ . This group also developed several possible industrial production techniques which may allow further cost savings.

### 1.2.2 The design of the Off-axis detector RPC's

Glass RPC's have been shown to be stable and reliable in more than four years of operation at KEK. It has therefore been decided to follow the BELLE design as closely as possible.

Each RPC consists of two glass plates, 3 mm thick held 2 mm apart. The 2 mm separation is ensured by a T-shaped gas seal that is inserted around the perimeter of the chamber and by a series of 2 mm wide long Noryl spacers positioned 20 cm apart. Each spacer extends from one side of the chamber almost all the way to the opposite side. Alternate spacers start on opposite sides of the chamber. This maze-like configuration, together with the positioning of the gas inlets and outlets on opposite sides of the chamber, ensures a uniform flow of gas throughout the chamber.

The BELLE chambers were built with 2 mm glass. The reason for proposing to use thicker, 3 mm, glass in this detector is that this allows to increase the separation of spacers from 10 cm to 20 cm, while still being able to withstand a difference between the internal and atmospheric pressures of up to 20 cm of water. Reducing the number of spacers has two advantages. It reduces the dead space, and therefore the inefficiency, caused by the spacers. It also greatly reduces the required manpower and time, and therefore the cost, to perform the difficult operation of gluing the spacers in place.

The other difference with the BELLE chambers is the use of the triangular corner pieces. These do not affect the internal working of the chambers while allowing for more robust gas connections and accurate positioning devices.

### 1.2.3 The performance of RPC's

The performance of RPC's has been studied in the laboratory using a cosmic ray telescope and a set of small size prototype chambers. Each prototype is  $25 \times 25 cm^2$  and is built out of two 2 mm thick glass plates. The 2 mm separation between the glass plates is ensured by the T-shaped gas seal that is inserted around the perimeter of the chamber and by a spacer that is positioned such as to run from one side of the chamber almost all the way to the opposite side. The gas inlet and outlet are positioned on either side of the spacer thus ensuring gas circulation throughout the chamber.

The trigger was provided by a three-fold coincidence of scintillation counters the size and position of which ensured that triggering particles traversed the

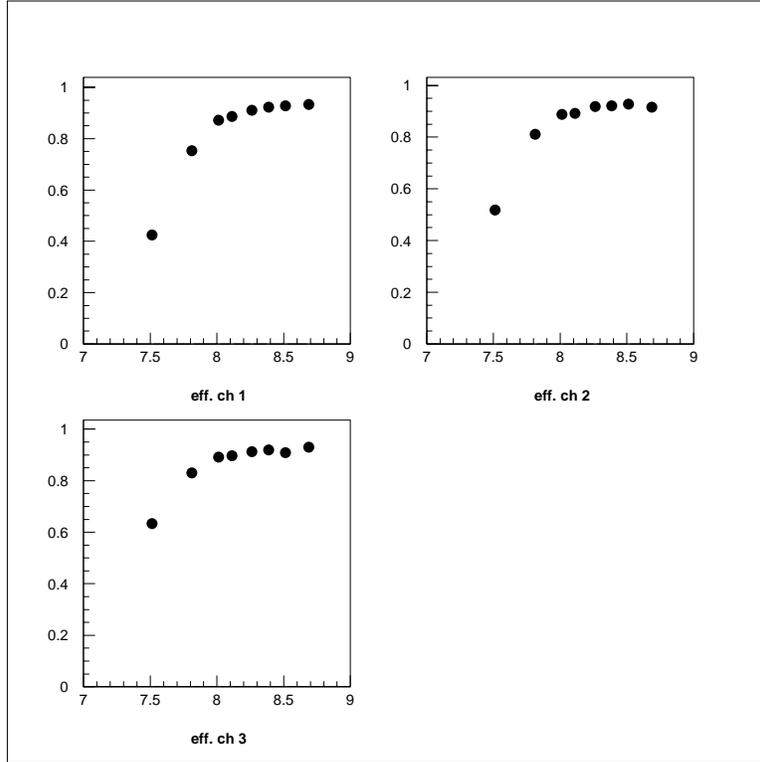


Figure 1.7: Efficiency as a function of high voltage for three chambers

chambers under study. Three chambers were stacked between the counters.

The efficiency of these chambers as a function of high voltage is shown in Fig. 1.7. It reaches 92% at 8.3 kV and remains flat for several hundred volts beyond this voltage. The dead space introduced by the spacer can account for about 1-2% out of the 8% inefficiency. In BELLE, in order to reduce the 8% inefficiency of RPC's, two RPC's were sandwiched between a single pair of readout planes resulting in each readout plane being sensitive to the sum of the pulse heights generated by the streamers in both RPC's. Furthermore the position of the spacers in the two RPC's were staggered so as not to overlap. A similar solution is envisaged in this detector with two planes of RPC's being positioned between two readout boards.

The pulse height induced by the streamer on the pad increases almost linearly with high voltage as shown in Fig. 1.8.

The dependence of the pulse height induced on the readout boards on the distance between the readout board and the RPC was also studied using the same three chambers. It is shown in Fig. 1.9. Increasing this distance from 0 to 9 mm results in a factor of two loss in pulse height. Note that in the configuration in

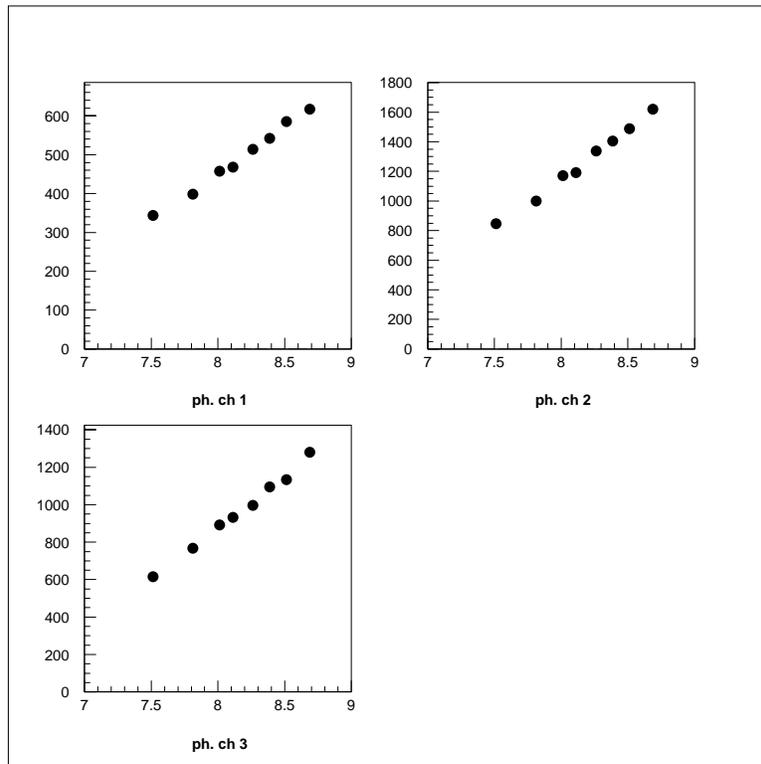


Figure 1.8: Pulse height as function of high voltage for three chambers

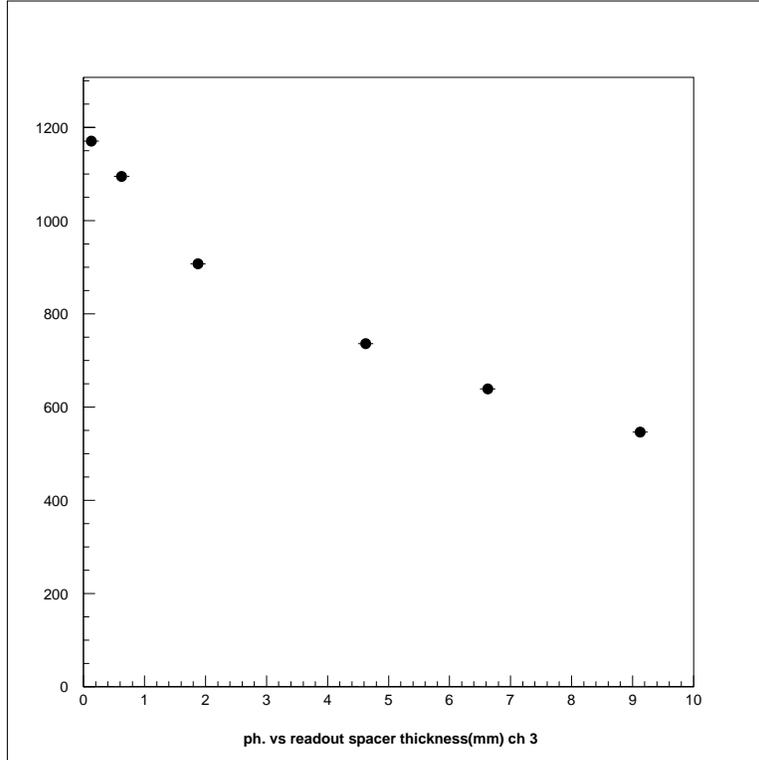


Figure 1.9: Pulse height as function of high voltage for three chambers

which two RPC planes are read out by a single pair of readout boards, each of the two chambers will be at this distance from one of the boards.

The crosstalk, defined in this instance as the number of times a particle gives a signal in two strips, the one it traverses and an adjacent one, was studied by using a chamber with a 3cm pitch strip readout instead of a single pad readout. This is shown in Fig.\*\*\* as a function of the distance between the trajectory of the particle and the edge of the adjacent strip. It goes from 100% when the particle passes just at the edge of the adjacent strip to 3% when the particle is in the center of the neighboring strip.

#### 1.2.4 Construction of Resistive Plate Chambers (RPCs)

RPCs are produced with a rectangular shape,  $284 \times 243 \text{ cm}^2$ .

Corners of each of glass plate are cut away, with the resulting discards in the shape of isosceles triangles, 5 cm on shorter sides, as shown in Fig. 1.10.

The cut out corners are replaced with an injection-molded noryl piece that acts as a gas manifold, Fig. 1.11 and has holes for positioning pins or through-

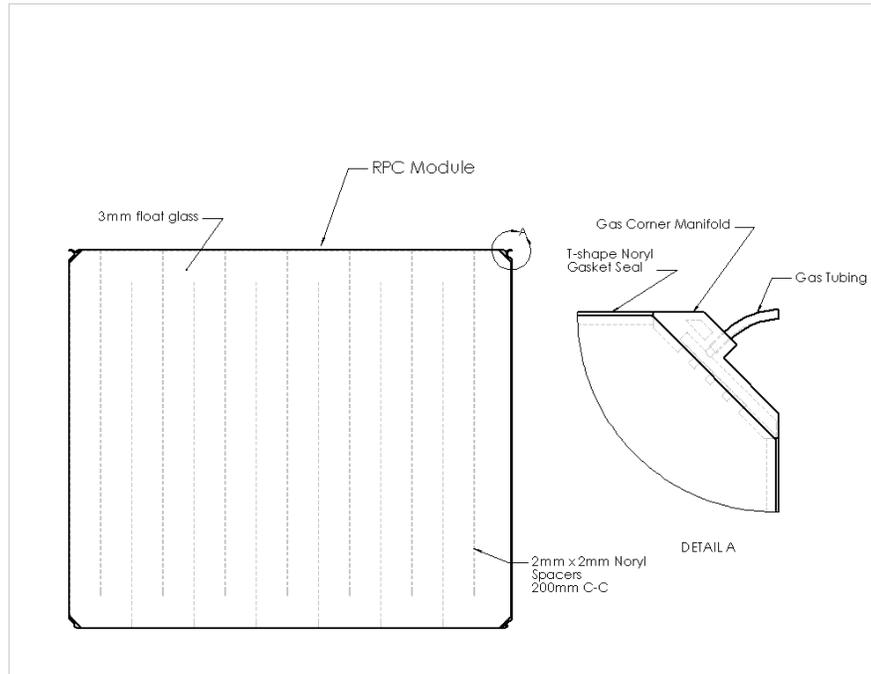


Figure 1.10: Glass RPC design with corner gas manifolds.

bolts, Fig1.12. RPCs are delivered with a thin sheet of plastic (0.5mm) cover on both sides to insulate the HV planes and to facilitate the handling.

The outside faces of RPCs are coated with a conductive acrylic paint, Stat-guard. Two insulated wire stubs are attached, one to each side. The wire is rated to withstand 20 kV. After installation on the readout board, the wires are spliced to a longer harness of 20 kV wires and routed to the outside of the RRA, where a solder connection to the high voltage C-W supply is made.

The injection-molded triangular gas manifolds are installed at the time when RPCs are assembled. Gas connections are made by gluing flexible tubing onto an injection-molded pipe stub. The glue will be a 5-minute epoxy. The gas manifolds also have holes for through-bolts and alignment/retention pins.



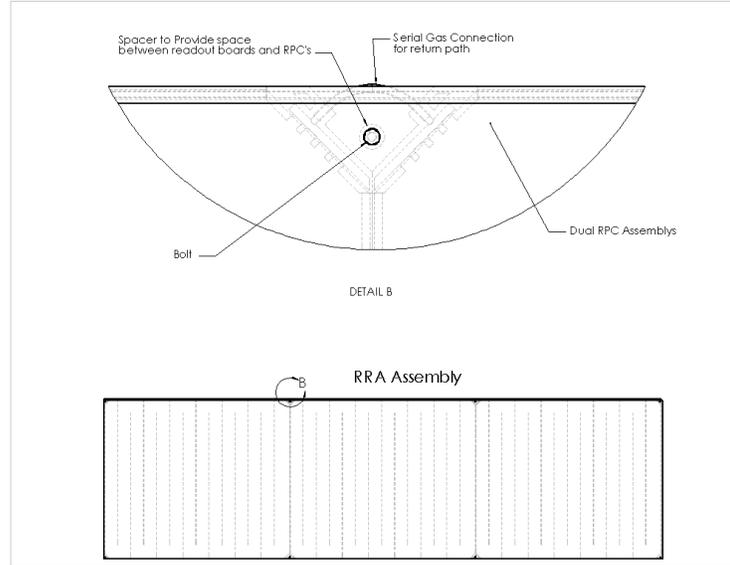


Figure 1.12: Assembly of tree RPC chambers bolted to the readout boards

### 1.3.2 RPC readout boards

Constructing RPC readout boards from the 2.5 cm thick sheets of absorber (particleboard) will maintain the uniformity of the detector and is cost effective. Each plane of RPC is sandwiched between two readout boards with the Cu readout strips facing inward. One board has 64 horizontal strips (3.80 cm pitch) and the other has 192 vertical strips (4.43 cm pitch), as shown in Figure 1.13. To create transmission lines, both boards have a solid sheet of Cu on the backside. We have decided to use copper as the conductor for ease in making large numbers of reliable electrical contacts with solder, conductive adhesives, or perhaps ultrasonic welding.

A source for Cu foil (1.34 m wide) has been identified. The least expensive unit area cost is obtained if the foil is purchased in a 17 micron thickness (a.k.a. 1/2 oz./sq. ft). We have contacted a number of firms who can laminate this Cu

<sup>1</sup>W. Riegler, C. Lippmann, R. Vennhof, Detector physics and simulation of resistive plate chambers, CERN-EP/2002-046, NIM A500(2003) 144-162, and references therein.

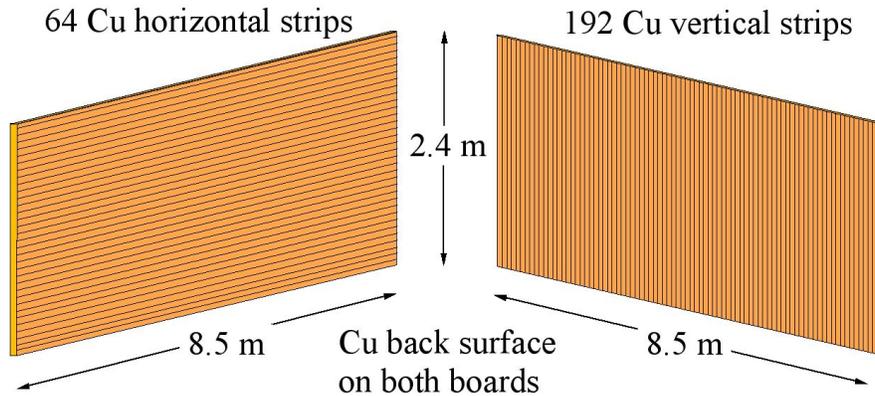


Figure 1.13: The readout boards required for each RPC plane.

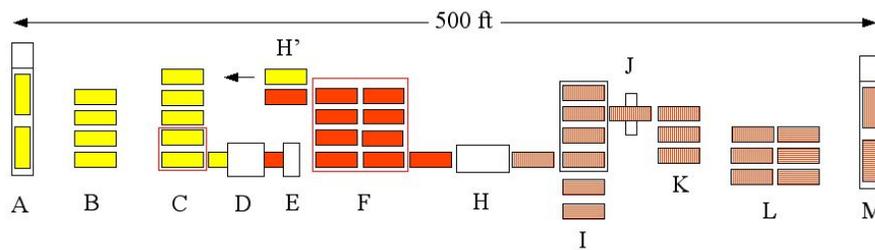


Figure 1.14: Readout board lamination and strip cutting production line.

foil to the 2.4 m wide particleboard surfaces and cut the strips. One company gave us a budgetary cost estimate, and a detailed sketch of a 500' production line, as shown in Figure 1.14.

Each day two truckloads of particleboard arrive at the production line (A) and two truckloads leave with finished boards (M). The steps and equipment required include: storage (B), unstack, pick and place (C), roller coating, facing with 2 Cu rolls, including a center seam applicator (D), slitter (E), dual pick and place, and glue curing station (F), FIFO to either a dual direction roller cutter (H), or cycled back for second side lamination (H'), stacker, pick and place, and QC station (I), bander (J), accumulator (K), finished and interleaved storage (L). The roller cutter would operate much like a ganged pizza cutter; however, the shape must be specifically designed to prevent bulging on the sides of the wedge cutter, as shown in Figure 3.

The company would purchase any needed equipment and setup the line in an available building. The line would operate over a 2.5 years and produce 60

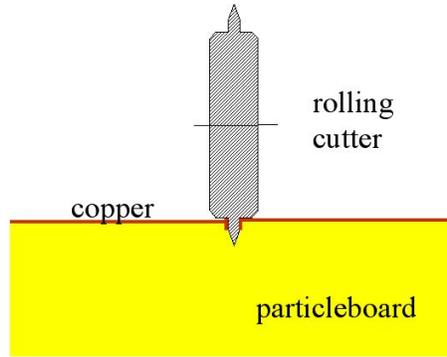


Figure 1.15: Detail of roller cutter shape.

boards/day, for a total of 28,800 boards plus spoilage and spares.

### 1.3.3 Signal Collection

The RPC signals are analyzed by discriminators packaged in a 64 channel chip (see electronics section xx). Discriminator chips are mounted on interface boards that are in turn mounted directly on the readout boards. Signals from the readout board strips are collected and transported to connectors on the interface board.

We propose to use flexible (flex) circuit boards and flat conductor cables as the collection and transportation

We will try to maintain the transmission line impedance of the readout strips ( $\sim 100$  Ohms) in the collection and transportation scheme. The extent to which this will be necessary or possible will be the focus of an R&D project.

A single-sided flex circuit board has been designed with 32 pads on the same pitch as the readout strips, as shown in Fig. 1.16 (not to scale). The pads are glued face down on the end of the readout strips with an adhesive (3M z-phase) that makes connections through the glue, but does not conduct between pads. Alternatively, solder or ultrasonic welding could be employed. The circuit has a 32 channel fan-in to a neck 6.5 cm wide. Mating to the conductors at the neck of the flex circuit, and permanently attached by the manufacturer, is a 32 channel flat conductor cable with 1 mm wide conductors on a 2 mm pitch. The flat conductor cable will be made in seven different lengths; six for the vertical strips and one for the horizontal strips. The flex circuits bend over the edge of the readout board, lie flat and are taped against its back side, as is shown in Fig. 1.17.

Separating the flex circuit from the back conductor is a dielectric sheet. The thickness of the dielectric is chosen to match the fan-in and cable impedance to the impedance of the strips. The cables must make 90 degree folds to reach the outer edge of the boards. In each fold it may be necessary to insert a conductor

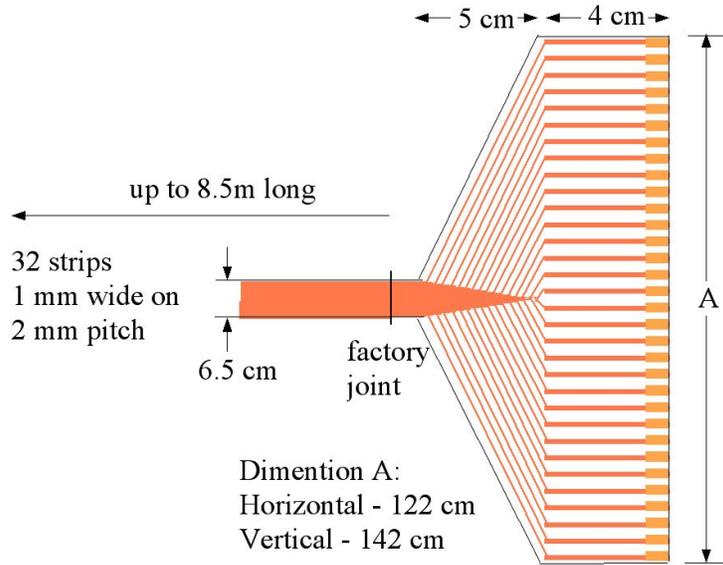


Figure 1.16: Signal collection flex-circuit and flat conductor cable

and (or) the proper thickness of dielectric to prevent an impedance mismatch. At the outer edge of the readout boards the flexible flat conductor cables will insert and lock into mating connectors on the discriminator interface cards. The flat conductor cable will extend beyond the end of the readout boards but will fold back into a 2.5 cm wide slot, created by attaching a another particleboard “spacer” on the back side of each readout board, as shown in Fig. 1.18.

This arrangement is designed so that electronics can be mounted and tested on the RPC detector package. Without modification, the package can then be inserted into an absorber module.

## 1.4 High Voltage Supply and Control

### 1.4.1 Overview

The high voltage system is composed of distributed HV supplies, with one HV supply per RPC. This amounts to approximately 104,000 individually controlled supplies, equipped with HV reference and current readback. The system is operated via a “slow control” serial network based on the CANbus commercial protocol. CANbus nodes contain multiplexed DAC and ADC modules to set RPC voltage and to read reference voltage and current. Current readback for individual RPCs is an important diagnostic of the operational state of an RPC.

In terms of the detector layout, each of the 1,200 detector modules has one

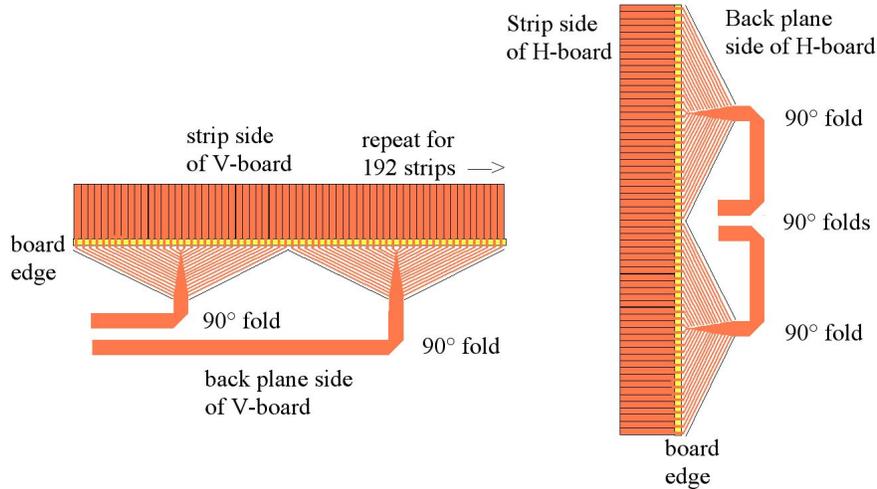


Figure 1.17: Routing of signals on back plane side of horizontal and vertical readout boards

CANbus node and 72 Cockcroft-Walton (C-W) high voltage supplies, with 6 C-W supplies per HV board. Each C-W supply operates with about 1 Watt of power, resulting in approximately 72 W per module. The CANbus node uses an additional 8 W, for a total power consumption of 80 W per module. One HV board provides voltage to one full plane of double-layered RPCs, for a total of 12 HV boards per module.

A list of the building blocks is provided below.

ITEM	LOCATION	Total Number in Detector
C-W supply	one of 6 on a C-W board	86,400
C-W board	one of 12 on a detector module	14,400
CANbus node	one per detector module	1,200
24 V power supply	one per 8 detector modules	150
PCI card	on C-W PC	3
PC	one, in control room	1

#### 1.4.2 High Voltage Generation

Six C-W HV supplies are housed on a single 4" x 12" HV board. The board powers one plane of RPCs. It is located on the outside edge of an absorber plane, adjacent to the RPC plane. HV is carried to the RPCs via insulated wires, rated at 20kV. Wires are soldered to the C-W board and to the RPC; no connectors are used. The wires are routed to the RPCs in a groove at the top of the RPC carrier board.

The C-W board communicates with the local CANbus node. Set points for

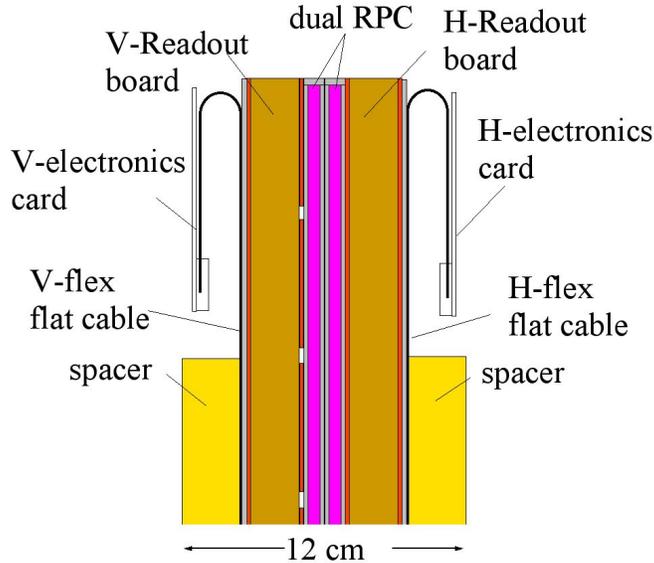


Figure 1.18: Routing of flat conductor cables to allow connection to discriminator interface cards

each of the six C-W supplies are provided by analog signals from the node. In turn, each C-W supply returns reference signals proportional to HV and the operating current.

In simple terms, a C-W supply is composed of diodes, capacitors, and transformer. Durable components are chosen. For example, although the capacitors operate at 200V the C-W boards use 500V-rated capacitors with a very reliable X7R dielectric. (Note: the troublesome capacitors on the ZEUS experiment used Z5U dielectric, now known to be rather unstable. Z5U was chosen because of its high dielectric constant, which made it easier to pack a large number of them in a small space.)

### 1.4.3 System Control

The system is controlled by a PC with three PCI cards (NI PCI-CAN/2). Each PCI card can communicate serially with 500 nodes via two CANbus controllers on the card. The CANbus node sets HV and reads back HV and current for all of the RPCs in a module. The node is a PC board that contains a CANbus processor and other electronics, including a multiplexed DAC and a multiplexed ADC. The processor communicates with the PCI card, executes routines and controls the multiplexed DAC and ADC modules.

Each C-W supply receives a command voltage from the multiplexed DAC to set the HV output. Two reference voltages, proportional to the high voltage

and to the current, are read back by the multiplexed ADC. This information is relayed to the PC for monitoring and the possibility of fine tuning the set point.

Physically, the node board has one connector for the CANbus serial communications bus, one connector for power input and twelve connectors to communicate with all of the C-W boards on a module.

#### 1.4.4 Power

The power consumption per C-W supply is calculated as follows. An RPC draws 1 uA per square meter under good conditions and up to  $\sim 5$  uA/m<sup>2</sup> before becoming inefficient. The RPC size is 6.9 m<sup>2</sup>, so the current will range from 7 to 35 uA. In addition the no-load current is presently 40uA (this value can be reduced). An average total current of 50uA is reasonable to expect, with possible surges up to 75 uA. The average power per C-W supply is  $\sim 400$ mW with a maximum of 600mW. If one includes inefficiencies, the resulting average power consumed is about 1W per C-W, with surges up to 1.5W.

One module consumes  $\sim 72$ W for C-W supplies plus  $\sim 8$ W for the CANbus node, for a total of 80W. Peak demand if all RPCs draw maximal current is 116W. A vertical stack of 8 modules draws 640W average and 928W peak. Therefore each vertical stack of 8 modules requires one 1kW power supply.

With a detector 75 modules deep, the number of low voltage power supplies is 150. The supplies are 1kW @ +24V.

## 1.5 Readout Electronics

### 1.5.1 Overview

When operated in streamer mode, RPC detectors produce a large pulse in response to the ionization within the gas. The signals are large so that a significant voltage (100 mV or more) can be developed across a 50 or 100 ohm resistor. Because the measurement of events requires only the observance of hits in the detector, it is sufficient to use a simple discriminator as the front-end electronics, without the need for additional amplification or signal processing.

To facilitate event reconstruction, the output of each discriminator would latch a timestamp. The timestamp is formed using local counters, which receive a common clock and counter reset signal from a global timing system. In this way, all timestamp counters across the detector are synchronized. When an RPC channel is hit, the data that is recorded is the value of the timestamp counter. The timestamp hits are stored in a local memory, and read out later. A block diagram of showing the functionality of the system is shown in Fig. 1.19. The resolution of the timestamp is determined by the clock speed, which might be 100 nS (10 MHz.) The number of bits in the counter is determined by the frequency of the counter reset, which might be 1 Hz.

Insert Functional Block Diagram

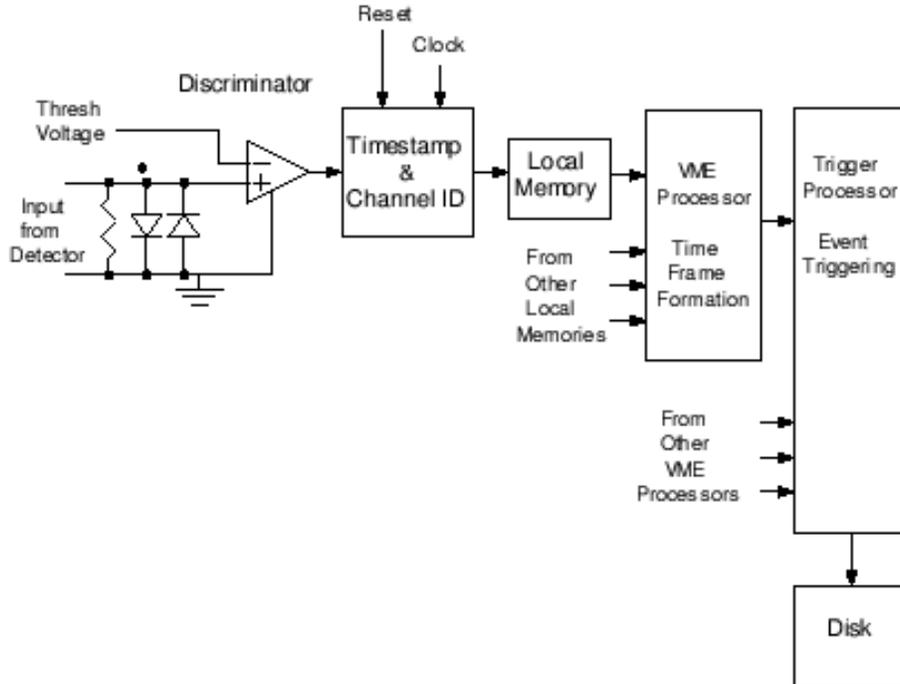


Figure 1.19: Functional Block Diagram

Because the data rate is low, it is envisaged that no trigger hardware is needed. Instead, the formation of a trigger and the analysis of events are done using a series of processors. This is similar to the data acquisition system of MINOS [reference the MINOS TDR]. The initial sorting of hits by timestamps is done using a VME-based processor in the front-end crate. The processor would form "time frames" using the time-sorted data. The time frames are then sent to a trigger processor, which receives time frames from the entire detector. The trigger processor runs algorithms that look for tracks and discard noise hits. Those events that pass are either written to disk, or passed to another processor for further analysis.

The functionality of the basic system described above would be configured into the components shown in Fig. 1.20. The basic components are: the Front End ASIC, which processes the detector signals and forms timestamps; the Data Concentrator, which coalesces data streams from the front end ASICs to reduce the number of readout boards; and the Data Collector, which is a VME board that receives the data streams from the front end, and makes data available for readout by the front end processor; and the Trigger Farm, which performs the event reconstruction, triggering, and event selection. These components are described below.

### 1.5.2 Front End ASIC

A goal in the electronics development is to make it low cost. Given the high channel count and relatively simple front-end configuration, it is practical to implement the functionality in a custom front-end Application Specific Integrated Circuit (ASIC). The discriminator, timestamp counter, and local memory are easily realized in silicon. A block diagram of the ASIC is shown in Fig. 1.21. The ASICs would be mounted directly on the detector.

The ASIC would have 64 input channels. Each channel is composed of a fully differential instrumentation amplifier, an optional preamplifier with shaping, and a discriminator, as shown in Fig. 1.22. There is a common threshold for all channels on the chip. Since the amplifier is differential, it may be used for either positive or negative input signals.

When a discriminator fires, the change in output state is clocked into a shift register at the fundamental clock frequency. The value of the timestamp register is also stored. At the output of the shift register, the decision is made to either write the data to a readout buffer, or have it rejected. The data is composed of the timestamp and the hit pattern. On-board logic can be configured to auto-accept any non-zero event, or perform more complicated accept criteria.

Once data is stored in the readout buffer, it is serialized, buffered, and transmitted out. An on-board UART controls the data transmission whenever the readout buffer is not empty. The readout buffer can store multiple events pending transmission. The output link runs at 100 MHz. An output word consists of 88 bits, which represents the state of the discriminators in one clock period. With control bits, the chip can transmit 1 event in 1 uSec.

### 1.5.3 Data Concentrator

It is expected that the event rate from the detector will be low. To reduce the cost of back-end electronics, the system would have an intermediate data concentrator that coalesces the data streams from the front end ASICs in an entire plane into one stream. A block diagram is shown in Fig. 1.23. The data concentrator would reside on the detector, close to the front end ASICs. Essentially, this device is a multiplexer, although it must add an identifier to each data stream. It also must have buffering and flow control. The realization might be achieved using either an FPGA or a custom ASIC.

An additional level of data may be possible by concatenating the output data streams from several data concentrators into one "super concentrator". The output would run at 1 GHz, and would use serial transmission over fiber. There would be one super concentrator per module.

### 1.5.4 Data Collector

The serial data streams from the detector would be received by custom modules that reside in VME Crates, called Data Collectors. A block diagram is shown in Fig. 1.25. It is a 9U by 400mm card that had 12 inputs for serial data.

The data is received and buffered, and written into one of two readout buffers. One buffer is made available for being read by the VME processor in the crate, while the other is used for writing new data. The state of the buffers changes at a set frequency, synchronized across the system, to facilitate the formation of "timeframes" of data. The Data Collector also provides control for the front ends, including the setting of threshold voltages, the fan out of clock signals, and diagnostics.

### **1.5.5 VME Crate**

There would be multiple Data Collectors in a VME crate, as shown in Fig. xx. The crate would also have a Timing Module for synchronizing the formation of timeframes of data. The Timing Module generates Interrupt Service Requests (ISRs) at a predetermined frequency. When a given ISR is received by the VME processor, it then reads data from the buffers on all of the Data Concentrators associated with that ISR. The next ISR would be generated to read from the other buffer. The VME processor collects blocks of data to form timeframes, which might be nominally 1 second worth of data. At the end of the formation of a timeframe, the VME processor would send the collected data to the Trigger Processor, where event reconstruction and triggering is done.

### **1.5.6 Physical Configuration on Detector**

Each detector module consists of 12 planes, where each plane has 192 vertical strips and 64 horizontal strips. The horizontal strips come out to the vertical sides of the detector. The front end ASICs for the horizontal strips would reside on a small printed circuit board on the edge of the detector. There would be one 64-channel chip per plane for the horizontal strips. The vertical strips would have signals brought from the top of the plane over to the side of the detector through the use of flex cables. In this way, all of front end ASICs would be located on the side of the detector, providing easy access for servicing. The vertical strips would be serviced by three 64-channel ASICs, for a total of four chips per plane.

Each plane would have one Data Concentrator. There would be one Super Concentrator per detector module. This would produce one serial data stream per module.

Each Data Collector has 12 inputs. It would require 100 Data Collectors to read out the 1200 detector modules. Assuming no limitations due to data rates or data transmission, this could be realized by having six VME crates, three per side.

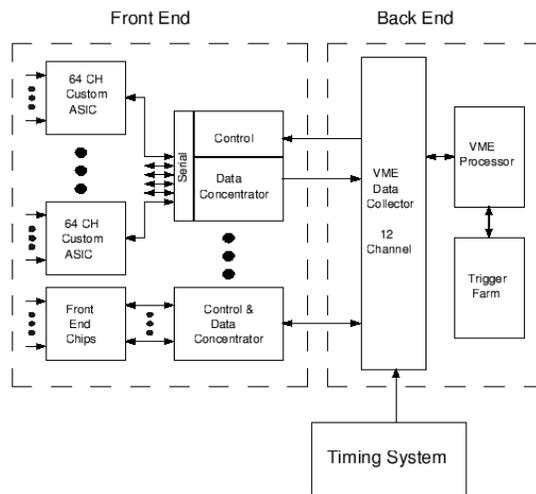


Figure 1.20: System Block Diagram

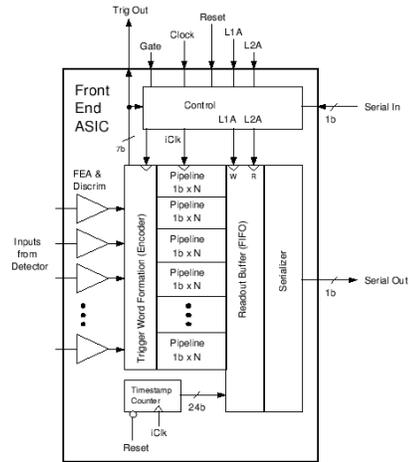


Figure 1.21: ASIC Block Diagram

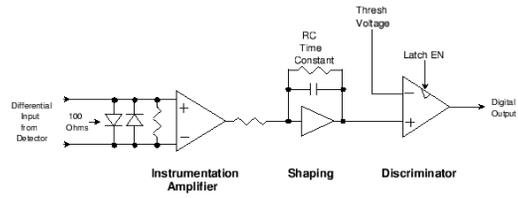


Figure 1.22: Front end amplifier

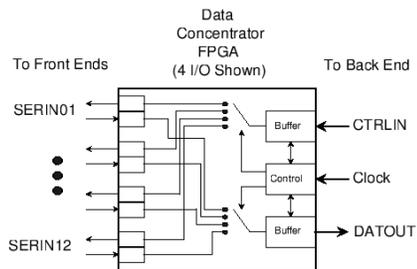


Figure 1.23: Data Concentrator Block Diagram

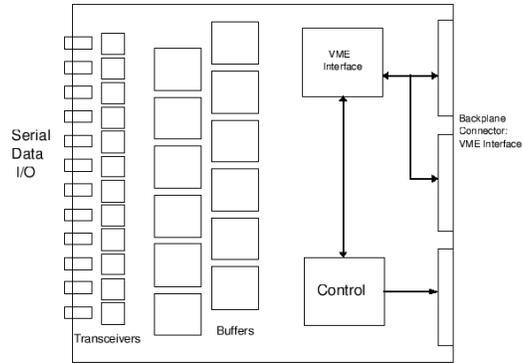


Figure 1.24: Data Collector Block Diagram

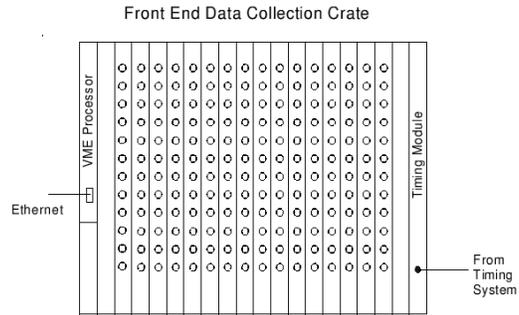


Figure 1.25: VME Crate diagram

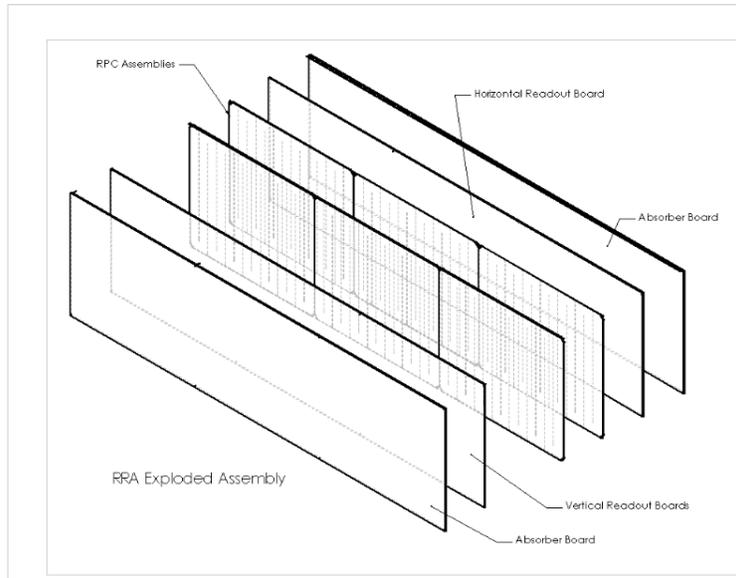


Figure 1.26: Composition of a RPC/Readout Assembly (RRA).

## 1.6 Absorber/RPC unit design and construction

### 1.6.1 Overview

There are 12 RPC/Readout board Assemblies (RRA) in each module. These, in turn, are separated by eleven 4" particle-board absorber planes and bounded by two 3" absorber planes at the ends. An RRA is composed of six RPCs, three adjacent in two layers, sandwiched between sheets of particle board outfitted with readout strips and ground planes. Another 1" particle board is attached to the outside of each of the two readout boards to protect the flexible circuit cables overlying the ground planes. The layout and assembly of these structures is shown in Fig.1.26 and described below.

### 1.6.2 Components

The major components of an RRA are: RPC chambers, a horizontal readout board, a vertical readout board and two absorber panels. Note that the readout boards are composed of absorber panels with strips of copper on one side and

a copper ground sheet on the other side.

### 1.6.2.1 Readout boards

The readout boards are made of particle board absorber material with dimensions 243 cm x 853 cm x 2.54 cm. A horizontal readout board has copper strips along the 853 cm direction on one side and a copper sheet (ground plane) on the opposite side. A vertical readout board has copper strips along the 243 cm direction and a copper sheet on the opposite side. Flexible circuitry is used to route signals from the readout strips to a compact edge connector, as described elsewhere in this chapter.

There are a couple of other differences between the vertical and horizontal readout boards. The horizontal readout boards support the RPCs with a built-in ledge along the bottom of the board. Also, gas tubing and high voltage wires are routed through or behind the top of the horizontal board. In the assembly process, RPCs are stacked on the horizontal boards and later covered with vertical readout boards.

The copper-strip side of a readout board is coated with a thin layer (0.5 mm) of plastic sheet to insulate the readout strips from the HV side of the RPCs, to protect the copper strips during the assembly process when RPCs slide over the strips and to facilitate the sliding process.

### 1.6.2.2 Absorber boards

The absorber boards are made of particle board with similar dimensions to readout boards, except that the absorber board attached to the horizontal readout board is 1.27 cm shorter (241.7 cm). The bottoms of the readout and absorber boards overlap exactly, but the top of the absorber board is 1.27 cm shorter than the readout board. This forms a slight depression that is used to route gas tubing and high voltage wires to the RPCs.

The absorber boards are connected to readout boards with screws that penetrate about halfway into the readout boards through the ground plane. Care will be taken to avoid using screws in areas where flexible cable is used.

### 1.6.3 RRA Assembly

The RRA assembly process starts with the following components already made:

- Vertical readout boards
- Horizontal readout boards
- RPCs
- Gas tubing harness
- High voltage harness

#### 1.6.4 Horizontal readout board units

To assemble a horizontal readout board unit (HRU), a horizontal readout board is first attached to an absorber board with screws, noting that the absorber is 1.27 cm shorter on the top side and 2.54 cm longer on the “outside” to protect the front-end electronic connections. Then a series of ledges is attached to the lower portion of the absorber board, with the requirement that the attachment is flush with the backside of the absorber (counter-bored surface). The ledge supports the readout board and the eventual RPC layers and vertical readout board unit. Finally, a set through-holes and alignment holes is drilled into the strip-side for eventual insertion of pins to align the RPCs via the injection-molded manifolds.

The HV and gas harnesses are attached to the HRU and, where appropriate, are routed through the RHU to the inside surface for attachment to RPCs.

#### 1.6.5 Vertical readout boards

To assemble a vertical readout board unit (VRU), a vertical readout board is first attached to an absorber board with screws, noting that the absorber is 2.54 cm longer on the “outside” to protect the front-end electronic connections. Care must be taken to avoid screwing through any flexible electrical circuitry.

#### 1.6.6 RPC Layers on HRU

The next step in the assembly process is to attach RPCs to the HRUs. To facilitate this process, a moveable table, equipped with height and tilt adjustment, is placed next to and at equal height with the supply of RPCs. One at a time, the RPCs are slid onto the HRU and placed in proper position, with the bottom of the RPC in contact with the support ledge and the alignment holes in agreement. Temporary alignment pins are placed in the holes, gas connections between adjacent RPCs are made to flow the gas serially and high voltage wires are spliced to the harness. Conductivity is verified and gas connections are checked against leaks.

The table is lowered to facilitate sliding of the next layer of RPCs in a similar fashion. Temporary alignment pins are replaced with the longer, permanent pins. Gas and HV connections are made and tested. Note that the gas connections, although serial in one plane, are totally independent between layers.

Next, the VRU is lowered onto the RPC-HRU assembly on the table. The VRU is supported on the bottom with the HRU ledges. It is tied to the HRU via through-bolts.

The RRA assembly is ready to be rotated 09 degrees to a vertical orientation for insertion into the pre-formed absorber module.

The RPC chambers are supported from the bottom by support shelf attached to the readout boards, as shown in Fig.??

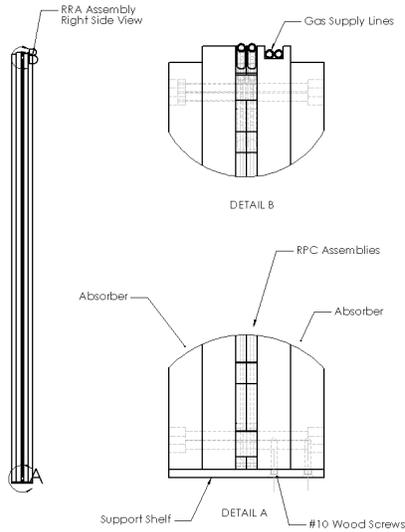


Figure 1.27: RRA assembly, side view showing in details the chamber support shelf.

### 1.6.7 HV, signal and gass connections

After the assembly of the RRA module is completed C-W supplies are mounted to absorber planes and the HV harness is soldered to the supplies. Readout front end chips are attached at this point, along with the gas connections to the supply & vent manifolds.

Gas supply lines are routed inside a cutout in the Horizontal Readout Unit, as shown in Fig. 1.28.

Front-end electronics chips are mounted on the sides of the readout boards and the signal cables are attached. The readout board are 1.27 cm shorter than the backing absorber boards, thus the absorber protects the electronics from accidental damage.

## 1.7 Detector construction

To complete the construction of the far detector in 4 years we have to make 88 working, fully tested RPC chambers every day. Four sites would likely be required to meet such a schedule. Even with four sites, the process will have to be highly automated. Adequate floor space to build, test and store modules prior to shipping will be required. Appropriate lifting fixtures for handling large sheets of glass will also be required. Once completed RPC chambers beginning to flow, we must build 16 RRAs per day. This task will require at least two sites with a fair amount of floor space as four assembly stations will be required at each site. To maintain this flow rate of RRAs, 30 readout boards and 16

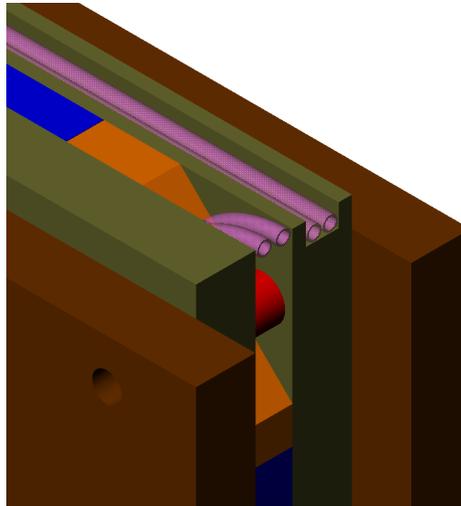
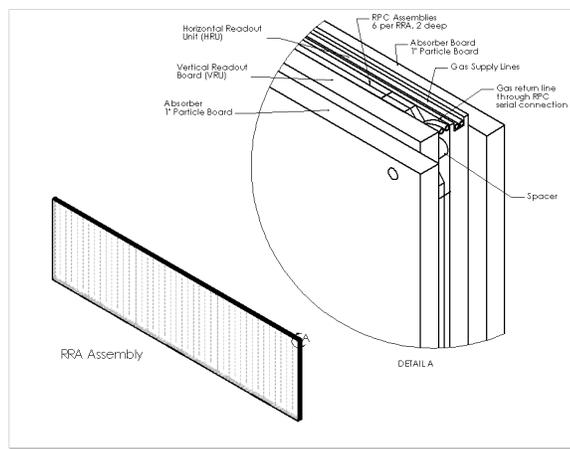


Figure 1.28: Corner of the RRA assembly showing the routing of the gas lines.

Cockroft-Walton boards will have to be provided each day. These parts could be fabricated elsewhere. The far detector contains a total of 1200 modules which requires an average of 1.2 modules to be produced each day. The module production consists of assembling the “toaster”, attaching the RRAs, attaching the module electronics and performing final module QC. Adequate floor space and a 20 ton crane will be required to assemble the modules and load them onto trucks for shipping to the final site. Two module assembly sites will likely be required. To minimize handling and shipping costs the modules should be constructed at the same sites where the RRAs are assembled. The absorber planes consist of 6 particle boards held together with glue and screws. The absorber planes will be assembled at the far detector site and loaded into the toasters as they arrive from the two factories. The absorber is loaded at the far detector site to keep the weight of the toasters shipped from the two factories below the threshold where special permits are required and additional costs are

incurred. Fig. 1.29 illustrates a possible flow of detector components.

## 1.8 Design of a Gas System

### 1.8.1 General Description

Gas will be stored and mixed at a central point. From there it will be distributed through manifolds to the twelve hundred modules. In each of the twelve hundred modules twenty-four branch lines supply three RPC's each. The return side will be collect the gas in manifolds arranged by layers, compress it and return it to the central supply. The design and fabrication would follow Fermilab PPD practices which significantly improved gas system reliability. The paper "Fixed Target Gas Systems" by Ted Gasteyer, 3/27/95 describes the features used to improve gas system reliability at that time. The nine mixing systems built at that time had almost no down time. Operations will be automatic and gas supplies will be large enough to run for months at the estimated leak rate. The pure gasses will be delivered and stored in tube trailers. For an estimated leak rate of 5%/day, an isobutene trailer would last 455 days, an R134a trailer would last 75 days and an Argon trailer would last 73 days. Flow balancing is not critical, but with flow restrictors the variation should be less than 15% between chambers. Since the gas is circulated there is no major cost incentive to minimize flow. Higher flow will speed up purging and drying. The gas system will mix, dry and circulate the mixture through the RPC's. Main materials will be stainless, copper or brass. Welded or brazed joints will be used wherever possible. Circulation and mixing will be fully automatic and status will be available on the web.

The following table summarizes the components of the gas system:

Item	Features	Total Number
Mixing systems	three flow meters, pressure control valve	2
module supply manifolds	w/strainer, flow transmitter	1200
RPC inlets	w/strainer, flow restriction	28800
RPC outlets	large enough for barometric pressure	28800
module return manifolds	w/pressure transmitter, relief, valves	1200
return compressors	dual compressor stations	10
gas storage	Mixture storage vessel	1
Mass spec gas analysis	analyzer with multiple sample points	1
moisture analyzer	local analyzers, one sample point	2

### 1.8.2 Gas specification and cost

The gas specification can be found at

"[http://www-off-axis.fnal.gov/detectors/RPC/gas\\_system/gas\\_system\\_specs.txt](http://www-off-axis.fnal.gov/detectors/RPC/gas_system/gas_system_specs.txt)".

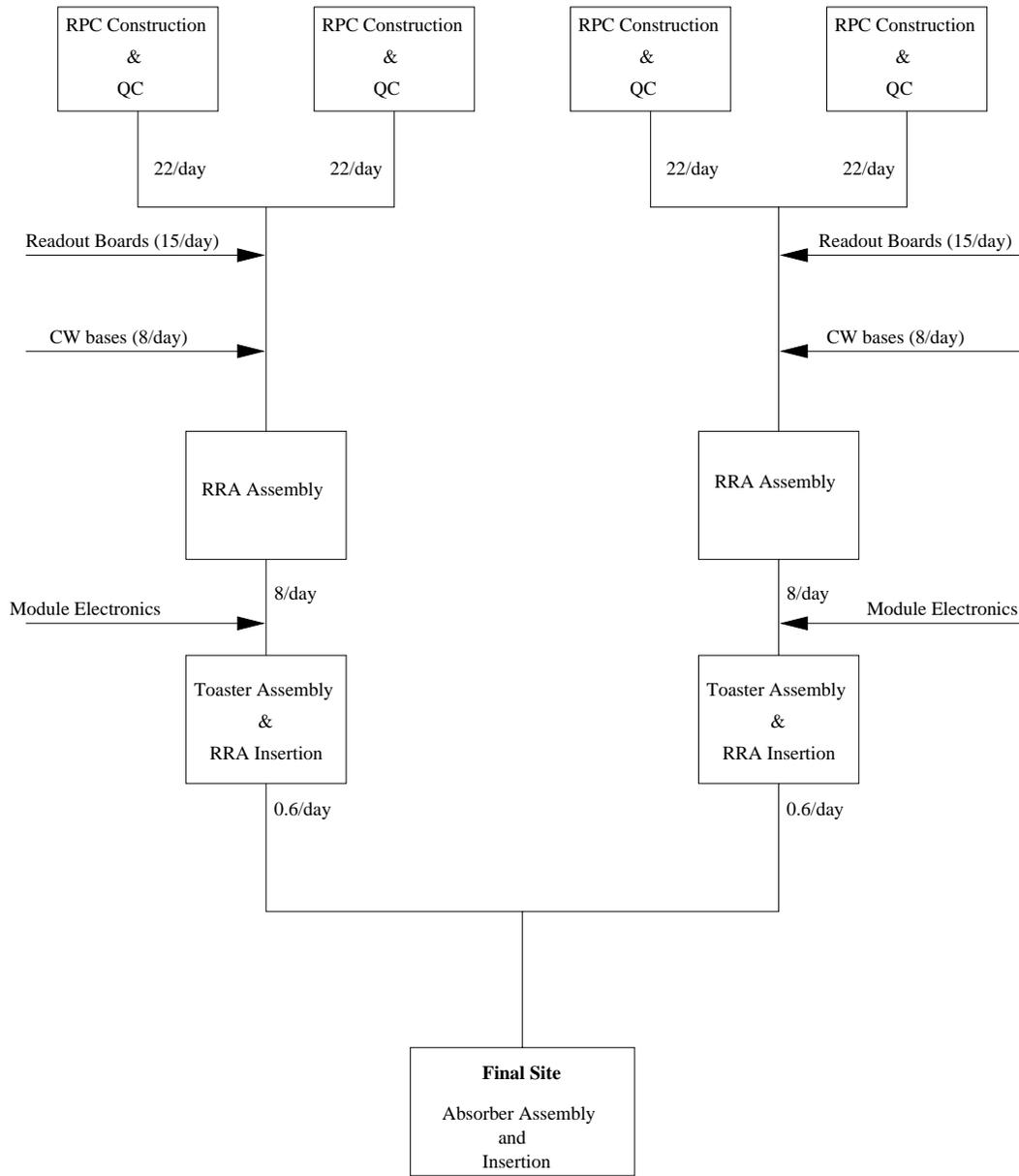


Figure 1.29: Flowchart of detector construction

Gas costs and regulations were summarized by Ivars Imblats at the Numi off-axis detector workshop at ANL, April 25-27, 2003. Studies will be done to determine the effect of air contamination.

### **1.8.3 Gas flammability**

The gas mixture is non-flammable. Sensors in the RPC supply gas will generate an alarm if the isobutane content is high. The area around the isobutane storage will be classified and constructed per NFPA 70, (National Electrical Code).

### **1.8.4 Glass thickness and spacer pitch**

Glass thickness is nominally 3 mm. For ASTM C1036 the thickness tolerance is from 2.92 to 3.40 mm. A study has been made of deflection and stress, " Study of RPC Glass and spacer parameters, RLS August, 2003.

### **1.8.5 Barometric Pressure**

Withstanding barometric pressure changes is a fundamental design requirement. Three parameters were used to define the system performance.

- Contain gas for barometric pressure within one inch of mercury of the mean. The gas storage will have enough capacity to handle this range. Only rarely will gas have to be vented.
- Contain gas for changes in barometric pressure up to 0.75 inches of mercury per hour. Almost all barometric pressure changes are slower than this. The pumps and tubing will be sized to handle the resulting flow rate.
- Relief capacity for reductions in barometric pressure up to 2.5 inches of mercury/hour. Relief devices will vent directly to the atmosphere.

Data to determine these specifications was taken from two sources: The National Climatic Data Center, International Falls, 2002 and from Soudan 2, 80,200 measurements 1989 to 2001. Further study is required including obtaining additional data from the National Climatic Data Center and the Soudan 2 barometric pressure design report.

### **1.8.6 Gas Distribution System**

Fig. 1.30 shows the general gas distribution system. Gas from the mixing system, storage and RPC return feed a buffer tank. Gas leaves the tank and is distributed into forty branches. Each branch includes a pressure control valve and is further split into thirty branches. The pressure control valve allows the flow to be varied in each of these banks of RPC's. Each of the twelve hundred branch lines includes a block valve, strainer and a flow transmitter. This is the inlet to a module of seventy-two RPC's.

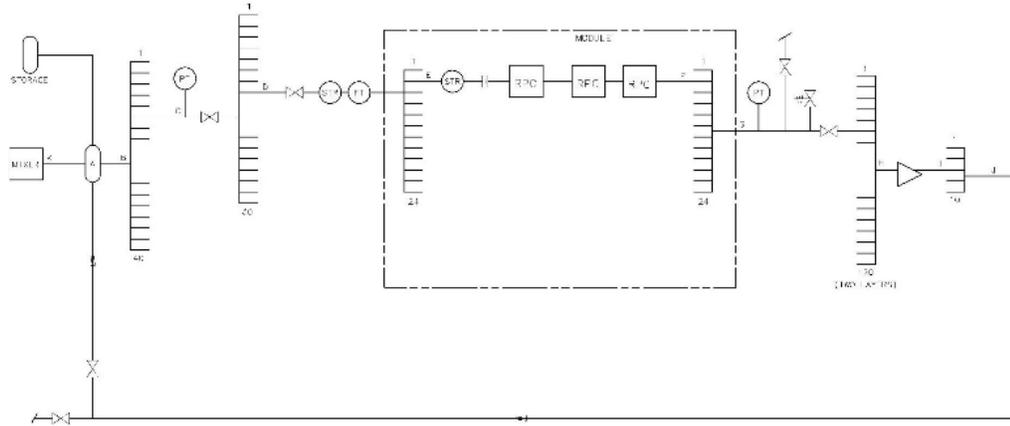


Figure 1.30: Gas distribution system.

At the module level the supply is split into twenty-four branches. Each of the branches includes a strainer and a flow restrictor. The flow restrictors should balance the flow within ten percent. The gas flows through three RPC's in series and is then combined with the other twenty-four branch lines in that module. Each module return line has a pressure transmitter, a vent valve, a relief valve and a block valve.

One hundred twenty module lines are combined to feed a compressor station. The discharge from the ten compressor stations will be returned to the buffer tank.

### 1.8.7 Gas Storage

A 500 cubic foot stainless steel vessel, compressors and valves will be used to store gas during normal barometric pressure swings. It will also provide a buffer to allow brief mixing and purification interruptions. Pressure in the vessel will vary between 0.5 to 35 psig.

### 1.8.8 Circulation

Gas will be circulated through all RPC's at the rate of two volume changes per day. The gas density results in a head of 0.25 inches of water for every ten feet in height. With a chamber design pressure of two inches of water, no more than two layers may be connected to the same compressor. A higher RPC design pressure would allow a smaller number of compressors to be used. The design for two inches of water would include ten compressor stations. For comparison

BELLE purged at the rate of one volume change per day and ran at one-half volume change per day.

Each station would have a primary and a backup compressor with automatic switchover. All wetted parts of the non-lubricated diaphragm compressors would be either stainless steel or PTFE. The capacity would be adjusted with speed control. Moisture is known to be detrimental due to the formation of hydrofluoric acid in the RPC's. Molecular sieve driers will remove moisture before it is supplied to the RPC's. Dual driers will be used so that one can be regenerated while the other is drying.

Two or three RPC's will be connected in series within containers or modules. Flow will be balanced between each group with uniform pressure restrictions, possibly capillary tubes like BELLE used. Each restriction will be preceded by a filter. During assembly the flow path through each flow restriction will be tested.

### **1.8.9 Mixing**

BELLE used mass flow controllers to balance the three gases. Similar mixing systems have been used at Fermilab for two, three and four component mixtures and have proven reliability. The flow range is too wide for a single set of flow meters and valves. To satisfy the wide flow range two mixing systems will be provided, one sized for filling and purging at 400 SCFH and the second for leakage makeup at 40 SCFH. The leakage rate is assumed to be 5% lost daily.

### **1.8.10 Materials**

Stainless steel pipe, tubing and valves with welded connections is the cleanest and most robust material selection. The installation cost estimate was too high, so less costly options are being considered including brazed copper tubing for the smaller branches of the system. A sample of layered plastic tubing will be tested for moisture desorption and permeation. Plastic material is inexpensive and flexible, but even if the permeability is acceptable, the reliability of thousands of fittings would have to be considered.

Stainless or copper tubing and fittings will be cleaned before assembly with detergent, rinsed with distilled water and alcohol. Connections that must be separated will be either quality compression fittings or O-ring fittings. Neoprene compatible with argon, isobutane, R134a, has good long term characteristics and a usable temperature range. It has low weight loss in vacuum and the permeability for nitrogen is good.

### **1.8.11 Pressure Relief**

Relief devices will be on the exhaust of each container or group of chambers. The pressure setting is two inches of water based on the BELLE RPC tests. The base design uses check valves with the spring removed. This has been done

in the past at Fermilab. The valves close reliably and will seal against internal vacuum. If a higher design pressure is chosen the setting will be increased.

Dual bubblers are less expensive but require accurate filling and more frequent checking. If the flow reversed they would require refilling. Bubblers become less practical if the design pressure increases.

### **1.8.12 Gas Analysis**

An ABB IMSQ4 mass spectrometer or equivalent will check for contaminants and the mixture ratio. Sensitivity depends on interference between gasses, but for nitrogen is at least 100 ppb. The mixture ratio from the analyzer will be used to automatically adjust the mixing system. A single analyzer will be connected to multiple sample points. The valves will sequence automatically through the sample points.

Since moisture is a known problem, moisture analyzers with at least 0.5 ppm sensitivity will be used. Long sample lines are detrimental to moisture analysis so analyzers will be located near the sample points. High moisture into the RPC's may be interlocked with high voltage.

### **1.8.13 Instrumentation**

Each module will have pressure and flow transmitters. With 1000 units, the models selected would be evaluated and tested carefully for price, accuracy and repeatability.

### **1.8.14 Controls and Alarms**

An industrial PLC (programmable logic controller) will contain the logic for mixing, circulation, alarms, etc. Fermilab has a lot of experience with these robust controllers. The controller will use the IEC 1131 languages for ease of configuration and debugging. It may be equipped with automatic backup processors, power supplies and other redundancies. The wiring, instrumentation and control logic will be documented.

A commercial HMI (Human machine interface) will interface between the PLC, gas analyzers and operators. It will record historical data and transmit alarms by email or telephone. Graphical displays of parameters and control settings will be available at the control room and other locations. A web server will be integrated with the HMI to provide access to real-time and historical data. Remote control will be strictly controlled but may be done on a limited basis. Remote alarms may be made by Email, telephone or through the web server.

A UPS (Uninterruptible power supply) will be used to keep the PLC, HMI and associated instruments running through short power outages and power surges. For longer power outages a backup generator will keep the gas system operational. The purpose is to avoid long cleanup times that could result if circulation is interrupted.

### 1.8.15 Procedures

There will be written procedures for assembly, leak testing, flow testing, normal and abnormal operations, maintenance, etc.

### 1.8.16 Prototype

A prototype container or module will be assembled and tested. The assembly will be evaluated for cost savings and assembly procedure before a final design is made. The gas system will be fully instrumented and tested for performance before a final design is made.

### 1.8.17 What-if Analysis

- How will RPC's be dried initially?  
Argon purge followed by circulation through driers.
- What about thermal expansion of pipe, tubing or gas?  
Flexibility calculations will be done. Care will be taken to keep stress on the RPC's low. Expansion joints or loops will be used where necessary.
- What if gas condenses in chambers?  
If the temperature is kept above -25F, the gas will not condense.
- What if the gas is spoiled?  
The contaminated zone will be purged until clean. The gas analyzer will be used to determine when the exhaust gas can be recirculated.
- What if mixture ratio needs adjustment?  
The mixture ratio will be measured with the gas analyzer. A portion of the gas will be vented. The makeup gas ratio will be automatically adjusted correct the overall mix.
- Effect of barometric pressure swings?  
Normally the RPC's will follow barometric pressure, operating at a small positive pressure. Compressors and valves will normally add or remove gas from storage. During rare, fast barometric pressure drops the module relief valves will operate.
- What if leaks occur during operation?  
A small amount of leakage can be tolerated. For example if five modules have substantial leaks, their exhaust flow can be vented rather than recirculated resulting in a loss of about 1%/day. Leaks causing serious contamination or loss of gas will be repaired. After repairs the affected area will be purged.

- How would a leak during operations be located?  
Block valves throughout the piping could be closed localize the leak using the gas analyzer and the pressure transmitters. It will be narrowed down to a manifold or container. Leaks will be found locally with thermal conductivity leak probes or bubble tests. Leaks in valves or connectors will be repaired.
- What if a module has to be isolated?  
Each container will be equipped with an inlet and outlet valve. The valves will be accessible outside the stack of containers.
- What if the gas contains water vapor?  
Molecular sieve adsorbers will remove water in the mixing system and the circulating gas.
- What if the gas has unknown or difficult to remove contaminants?  
Contamination is minimized by material selection, cleaning and leak testing. One solution is to vent a portion of the gas. For example, if a contaminant adds 10 ppm to the gas in one pass, then venting 5% of the circulated gas will limit the contaminant to 200 ppm.

## 1.9 Cosmic Rays Background and a Veto Shield

The off-axis detector will be operated on the surface and therefore must cope with the cosmic muons-induced backgrounds. They are discussed in a separate section of this proposal. General considerations indicate that one should expect vanishingly small number of cosmic-rays-induced events which can be classified as signal events.

High granularity of the proposed detector offers additional protection against unforeseen, conspiratory coincidences of backgrounds. The detector plane is subdivided into 16 independent modules, 8 in vertical and 2 in horizontal direction, thus a probability of a random coincidence of reduced by an order of magnitude.

Yet another protection will be provided by a veto shield. It will be constructed from two layers of RRA's of the same construction as the main detector, separated by 30 cm, and positioned on top of every module in a top layer of the detector. The signals will be readout at the side of the detector in a manner identical to those in the main detector.

## 1.10 Near Detector

Experimental determination of the NC and  $\nu_\mu$  CC induced backgrounds as well as a measurement of the  $\nu_e$  component of the beam requires a near detector of

the same granularity to be exposed to the NuMI beam at some location(s) on the Fermilab site.

The near detector will be constructed as a stack of 6 modules of the same construction as the far detector modules arranged in 3 walls, two modules high. Due to space limitations of the near NuMI hall the modules will be only 2/3 as long as the far detector modules: they will be 5.69 *m* long, 2.438 *m* high and 2.6 *m* deep.

Access shaft to the near NuMI hall limits footprint of the objects which can be installed underground, therefore the absorber plates as well as the RRA's will be lowered separately and assembled underground into a final module.

A detector with the same granularity as the far detector will, in the near position, detect a sum of the NC-induced background and the  $\nu_e$  component of the beam. These two components scale, in general, differently from the near to the far position. It is, therefore, very important to be able to separate these two components.

The NC-induced background consists of the events with energetic  $\pi^0$  produced in the final state. Relatively coarse longitudinal sampling, dictated by economy, does not allow detection of the conversion points of gammas from the  $\pi^0$  decay. We propose to augment the near detector with two additional 'walls', two modules high. These modules will have the same size as the 'standard' near detector modules, but they will have improved (reduced) sampling frequency. The modules directly upstream of the near detector will contain only RRA assemblies, thus having the sampling twice as good as the near detector. This will be a 'good resolution' section. The modules of the most upstream wall of this detector, the 'high resolution section' will contain only glass RPC's with no particle board absorber. The chambers will be sandwiched between two, aluminium skinned foam insulation boards. The sides of the foam board facing the chambers will be cut into 3 *cm* strips, vertical and horizontal, to provide signal readout. These strips in conjunction with the aluminum skin on the other side of the board acting as a ground plane form an excellent transmission line.

An example of a NC event with energetic  $\pi^0$ , detected in such a detector is shown in Fig. 1.31

A superb spatial granularity of the high resolution section of the detector is evident. This detector samples the final state particles with frequency of 0.05  $X_0$  and 1.4 *g/cm*<sup>2</sup>. This granularity will approach that of bubble chambers, whereas the NuMI beam intensity exceeds that of the old days neutrino beams by several orders of magnitude.

The high resolution section of the near detector will offer an opportunity to address many questions of poorly known neutrino physics at low energies. Last but not least, high statistics samples from this fine granularity detector will provide an essential calibration sample for modelling of low energy neutrino interactions.

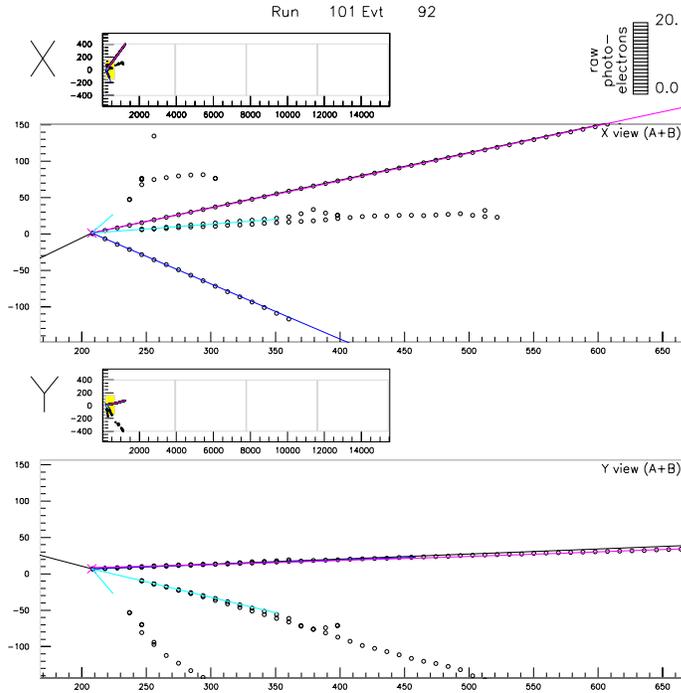


Figure 1.31: A neutral current interaction of  $2 \text{ GeV}$  neutrino with an energetic  $\pi^0$  as detected in the high resolution section of the near detector. Cyan lines indicate the direction of gammas emitted in the  $\pi^0$  decay. An enlarged section of the detector shows a volume of  $1.5 \times 1.5 \times 6.5 \text{ m}^3$ . This volume is larger, along the beam direction than the depth of high resolution section. The high resolution section will provide the topological information about the vertex part of the interaction, whereas the downstream sections will be used to measure provide measurement of the energy (range) of particles produced.

## 1.11 ES&H

There are several ES&H issues to consider during construction of the detector and they will be discussed in turns:

### 1.11.1 Fire

The detector's principal component is wood and represents a substantial fuel load at any module fabrication site as well as at the final location. Assembly methods chosen must make sure ignition sources in the module construction areas meet code. It may be necessary to paint the completed assemblies with fire retardant paint to limit their flammability. Housekeeping will be important because sawdust is more flammable than the actual panels.

### **1.11.2 Lifting heavy loads**

At every stage of construction it will be necessary to include commercial or specially designed lifting fixtures to handle the wood panels, glass plates, and the finished modules. All of this fixturing must meet the requirements of the OSHA standards. These fixtures will include vacuum fixtures for handling the glass, and container style lifting fixtures for the modules. Rigging procedures will be documented and reviewed in advance of construction and operations. Operators will have to be trained in the proper use of the hoisting equipment.

### **1.11.3 Glass handling hazards**

Handling thousands of square meters of glass is potentially a hazardous business. One estimate mentioned by a vendor was that breakage could be as high as twenty percent for very thin sheets. While this is a very high estimate because the present RPC design calls for thicker glass, procedures must be worked out to protect workers from the occasional broken pane. Here we will need to investigate the procedures and equipment used by large glass making companies to protect their employees. Special personal protective equipment will also likely be required.

### **1.11.4 Oxygen Deficiency Hazard**

For such a large detector the inventory of gas is significant. Standard Fermilab ES&H rules will be followed to minimize this hazard at every location, including all gas storage and mixing areas. Additionally it will be necessary to address the hazard in a situation where a module at the bottom of a stack will need to be removed for servicing.

### **1.11.5 Fall Protection**

Because of the height of the detector fall protection must be provided should there be any need to work on the detector stack. This might include railings and certainly will require harnesses and lanyards compliant with OSHA regulations. Crane cages, if required to lift personnel to the top of the detector, must be certified for that service. The present design does not include any need for working on the detector stack for operations or maintenance. Interim precautions will be needed as the detector is stacked up during initial assembly or for removing a bad module. This is because it is necessary to get to the top of a module to (un)attach the swivel hoist rings for lifting the module.

## **1.12 Operation and Maintenance**

Maintenance of the detector is normally routine monitoring of the gas system for inventory of gas, purity, and chamber flow rates. Inventory of the gas will also

be used to detect gross leakage in the chambers. All of the critical parameters of the gas system will be available for remote monitoring and alarming.

Electronics failures will be dealt with by substituting spares and making repairs to broken equipment off line. Sufficient spares will be needed to cover cycling seriously malfunctioning electronics out to off site repair facilities where the equipment originated, and the experts reside.

### 1.13 Installation of the detector

Finished module weight has been calculated at about 43 tons. This is too heavy to transport over the road without special permits and also too heavy for most of the assembly sites to be able to handle. To compensate for this, modules will be produced as incomplete “ containers” which are substantially lighter. They will not contain the RPC detectors or all of the absorber material. These could be manufactured locally or more likely at other sites and shipped in to the detector location. RPC’s will be manufactured at remote sites and shipped in for final assembly of the modules. At the detector site the modules will be assembled and tested before being installed.

For assembly of the modules a finished box will arrive from a remote assembly site. To that box planes of particleboard and RPC’s will be added to fill the box. These will be shipped in flat from a different factory site. To do this a special lifting fixture(s) will be required that can lift a plane to vertical and then install it in the slots in the box. After the slots are all filled then the gas manifold is attached and the electrical connecting wire are added for the readout signals and for the Cockcroft Walton high voltage power supplies.

Testing of the modules will include the following:

- After assembly the RPC’s will be pressure tested for leaks. They will also need a flow test to ensure that the tubing to each set of chambers is clear.
- A high voltage test will be done to ensure that the chambers have not developed problems in transit.
- Final testing will include a test of the module in position looking at cosmic rays. It will be necessary to stack the modules in such a manner that other modules cover up no module until this test is complete. This can allow it to be removed for any needed repairs before it is buried under other modules.

The detector is assembled as stacks of modules. The final detector is 2 modules wide by 8 modules high by 75 modules deep. In the initial stacking the modules will be placed such that after a few days the working face of the detector is stepped like stairs. This will allow the final testing to proceed without burying an untested module.

Columns along each side of the detector footprint will support the gas manifolds and signal and power cables. All of this will be assembled before the

detector stacking begins. Each side of the detector will also have an aisleway just outside of the columns wide enough to allow a manlift to operate. The manlift will be used to make all of the electrical and gas connections as the detector modules are added.

The present plan for lifting the modules is to use a spreader bar and four swivel hoist rings. Each module has corner blocks at the top drilled and tapped for the hoist rings. After the module is placed in position the hoist rings are removed and tapered pins are screwed in the same holes. These pins match the holes in the bottom corner blocks of the modules and are used for alignment as the modules are stacked up. Spreader bars as described above are commercially available. Fermilab has also produced such fixtures in the past.

## **1.14 Detector Enclosure, Infrastructure, Access to Detector**

We have completed two design studies on possible detector enclosures for an Off-Axis experiment. The first study was sponsored by the University of Minnesota and was performed by CNA Consulting Engineers with subcontracts to Dunham Associates and to Miller-Dunwiddie Architects (1). This CNA study focused on a cut and cover approach in bedrock with a 10-meter overburden as a first guess at a possible required cosmic ray shield. The second study was done by the Fermilab Facilities Engineering Services Section (2) and focused instead on no overburden on an above-grade building with a minimal excavation just down to bedrock to ensure the 50 kilotons is sitting on a solid surface.

While the two studies had different goals, they did agree with each other in cost at the 20% level when the Fermilab surface design was compared to a similar subsection of the Minnesota design done by Miller-Dunwiddie (3). In addition, both designs had common assumptions about the general site, for example including modest costs for short roads connecting to existing roads. Not all sites under consideration satisfy these assumptions. For the base designs being described here, one must scale either building design to reflect changes in the size of the detectors from the time of the studies to the time of this proposal. The Fermilab design in particular contains crude scaling arguments for just this purpose, allowing scaling for different detector widths, lengths and heights.

For the RPC base design described here, the detector will occupy a footprint that is 17.1 meters wide, 233.1 meters long, and 19.5 meters high. Since each of the 1408 modules in the detector weighs about 40 tons, the building must have 50 ton crane for assembly and possible repair of the modules. Stacking the modules requires an additional 5 meters clearance between the top of the detector and the crane hook (for one 2.45 meter high module plus an assumed 2.55 meter vertical space for a lifting fixture). Another few inches may be required for a carpet of RPCs to lay on top of the stack for cosmic ray veto / identification. Another 8 meters of vertical height are required for the crane bridge and for the roof trusses (4).

In addition the RPC design requires about 100 square meters for a gas mixing and distribution system and about 100 square meters of office/tech space. It is assumed that these areas are at grade, accessible through simple roll-up doors to outside roads. Incoming modules will not be complete, but it is assumed that the modules and the incoming stacks of RPC assemblies can initially be stacked all along the floor of the hall for final assembly. Final assembly of modules would take place at multiple stations all over the hall, and completed modules would be staged into the final stack, reducing the assembly and parts storage area as the detector grows. A residual small staging area should have space for several modules, allowing repairs on-site. Spare modules are assumed to be part of the original stack – that is, if an interior module must be pulled out for repairs, then a module from the final stack along the beamline will be substituted.

During and after assembly the detector will require access to both sides of the long (233 meter) dimension of the detector along the line of the neutrino beam. We propose two lanes on each side of the detector. The outside lane would be about 1 meter wide and primarily for personnel access. The inside lane next to the detector would be reserved for scissor-lift or boom & bucket devices or a warehouse distribution system on rails (see Fig. 1.32) allowing a person to touch every square inch of the outside surface at chest height for installation, debugging, and maintenance of the front-end electronics, high voltage, and gas systems. This lane would be approximately 3 meters wide. These lanes could be separated by a line of expressway median blocks with access between the lanes at the block junctions. The access lanes add about 8 meters to the width of the building.

Estimates for these access systems are needed and should be documented here.

Overall we need a surface building that is 25 meters wide, (233 + 4 + 4 + 9) meters = 250 meters long (detector + gas + office + staging), and 33 meters high. To estimate the cost, we scale from the Fermilab design which was 33.5 meters wide, 167.6 meters long, and 39.6 meters high, following the prescriptions given in the Fermilab FESS documentation (5). In addition, we have to add a complete HVAC system and a 50-ton crane to the base Fermilab design. This gives the following estimate:

Item	Estimate in \$ M
Base Fermilab building at grade	17.5
Scale width down from 33.5 m to 25 m	- 3.8 (27.9 ft * \$ 135 K / ft )
Scale length up from 167.6 m to 250 m	+ 6.7 (49% longer, so 1.49 * (17.5-3.8))
Scale height down from 39.6 m to 33 m	- 2.3 (ref 2, Appendix E)
Add HVAC system with 23 deg C +/- 2 deg	+ 1.5 (scale U of Minn * 2)
Add 50 ton crane	+ 1.4 (see ref 2, Appendix D)
<b>TOTAL</b>	<b>\$ 21.0 M</b>

References:

1. Report for Off-Axis NuMI Neutrino Detector, U of M Project No. 298-03-1113, January, 2003.

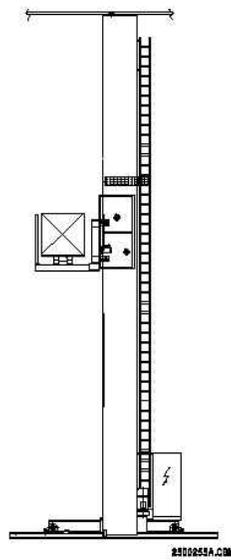


Figure 1.32: Possible access vehicles.

2. Off-Axis Detector Enclosure Design Study Report, Fermi National Accelerator Laboratory, FESS Engineering Project No. 6-2-22, June, 2003. Also available as Off-Axis Note #9.

3. see reference 1, pg 25, see also J. Cooper talk at ANL workshop in May 2003 available on the Off-Axis website.

4. see reference 2, Figure 8 in Section 5, page 13.

5. see reference 2, Section 1, page 2.

## Chapter 2

# Analysis and Physics capabilities

### 2.1 The generated event sample

The generation of Monte Carlo events and their reconstruction is described in [13]. Some of the studies presented in this chapter are described in [14]. The basic geometry, Fig. 2.1 used consisted in the following sequence of material:

- **zboard** cm of particle board,
- a glass RPC with X and Y readout, amounting to 5% of a radiation length..

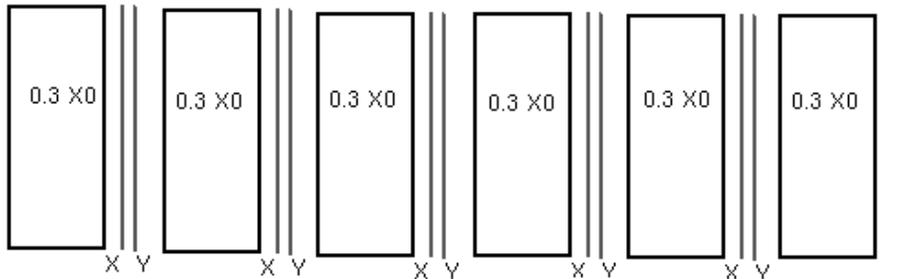


Figure 2.1: An example of the distribution of absorber and x,y readout planes

Particle board has a density equal to  $0.7 \text{ gm.cm}^{-3}$  and a radiation length of \*\*\*\*. For technical reasons it was approximated in GEANT by a mixture of air and plastic in the proportions of 5cm of air for 12.5cm of plastic.

Event samples with three different absorber thicknesses between active read out planes (RPC's) were studied: 17.5%, 30% and 60% of a radiation length. These are referred to, respectively, as the 6CM, 12CM and 24CM samples according to the approximate thickness of particle board they represent.

Furthermore, by ignoring the Y read out in the odd planes and the X readout in the even planes, a detector with alternate X **OR** Y readout in successive planes could also be studied. This was done for the 30% radiation length sample and is referred to as XORY.

The antineutrino studies which were also made with a 30% radiation length sample are referred to as 12BAR.

Several readout strip widths were studied.

For each of the geometries studied, charged current (CC) and neutral current (NC) interactions for both  $\nu_\mu$  and  $\nu_e$  were generated. The  $\nu_\mu$  interactions were used to study the background. The  $\nu_e$  interactions were used to study both the intrinsic  $\nu_e$  background present in the beam and the signal from  $\nu_\mu \rightarrow \nu_e$  oscillations. Since the  $\nu_\mu$  energy spectrum is sharply peaked at low energy and has a long tail, the events were generated in two stages: flat in energy between 1-3 GeV, and again flat in energy between 3-20 GeV. This resulted in a more optimum use of computer time. During the reweighting process the different numbers of events per GeV in the two energy intervals were taken into account. The reweighting also took into account the  $\nu_\mu$  and  $\nu_e$  energy spectra at the detector location, computed with the beam simulation program [15].

It should be noted that the background from the minor components of the beam (anti neutrinos in neutrino running) was not included in these calculations except in the section dealing with the comparison of neutrino and antineutrino running. Whereas the contribution of  $\bar{\nu}_\mu$  and  $\bar{\nu}_e$  in neutrino running is negligible at the 5% level, that of  $\nu_\mu$  and  $\nu_e$  in antineutrino running is indeed important and cannot be neglected.

## 2.2 The beam spectra and oscillation parameters used

In the subsequent analysis the detector was assumed to be located 10km off-axis at 732km. The beam spectra used to weight the events are in the form of arrays of 1000 bins of 20 MeV between 0 and 20 GeV.

The files used are:

- $\nu_\mu$  spectrum:

This file was used for three different purposes:

- It was used to weight the generated  $\nu_\mu$  CC events in order to study the background from these events. However, since the  $\nu_\mu$  spectrum at long baselines is depleted through oscillations to  $\nu_\tau$ , for this source of background, the weight read from the file was multiplied by the survival probability for a  $\nu_\mu$  at that distance and energy:

$$1.0 - \sin^2 2\theta_{\mu\tau} \sin^2 \frac{1.27\Delta m^2 L}{E_\nu}$$

with

$$\sin^2 2\theta_{\mu\tau} = 1.0 \quad \text{and} \quad \Delta m^2 = 2.5 \times 10^{-3} \text{ eV}^2.$$

- It was also used to weight the generated  $\nu_\mu$ NC events to study the background from this source. No survival probability was needed here since  $\nu_\mu$ NC and  $\nu_\tau$ NC events are identical.
- Finally it was used to weight the generated  $\nu_e$ CC events in order to study the  $\nu_\mu \rightarrow \nu_e$  signal events. Here the weight read from the file was multiplied by the  $\nu_\mu \rightarrow \nu_e$  oscillation probability, taken to be:

$$\sin^2 \theta_{23} \sin^2 2\theta_{13} \sin^2 \frac{1.27\Delta m^2 L}{E_\nu}$$

which becomes for  $\theta_{23} = 45$  degrees, and  $\sin^2 2\theta_{13} = 0.1$  (the CHOOZ' limit):

$$0.05 \sin^2 \frac{1.27\Delta m^2 L}{E_\nu}$$

- $\nu_e$  spectrum:

This was used to weight the generated  $\nu_e$ CC events in order to study the background from the intrinsic  $\nu_e$  in the beam.

When running at a yearly rate of  $4.0 \times 10^{20}$  protons on target the  $\nu_\mu$  file yields a rate of **107.594**  $\nu_\mu$ CC events per kiloton.year and the  $\nu_e$  file of **2.177**  $\nu_e$ CC events per kiloton.year.

Similarly for the antineutrino run the files used were the  $\bar{\nu}_\mu$  and the  $\bar{\nu}_e$  spectra with corresponding normalizations of **32.378**  $\bar{\nu}_\mu$ CC events and **0.707**  $\bar{\nu}_e$ CC events per kiloton.year.

## 2.3 The reconstruction of events

The method used was that of the Hough transform. It was applied separately in each view. The straight line with the largest number of hits within a tolerance of 15cm was found. These hits were then fit to a quadratic expression to take into account any curvature arising from scatterings. The resulting track was taken as the electron candidate.

The following variables were defined:

**ang**, the three-dimensional angle of the candidate electron with respect to the beam.

**tothit**, total number of hit strips in the event, a measure of the total energy of an event.

**ensumht**, total number of hit strips associated to the electron candidate, a measure of its energy.

**why**, the fraction of the event hits associated to the electron candidate.

**chimax**, the maximum of  $chix$  and  $chiy$ , the  $\chi^2$  of the fits to the electron candidate track in the x and y views.

**peet**, the overall net transverse momentum of the event, calculated as the sum, over all the hits in the event, of the sine of the angle subtended by each hit at the upstream-most hit in the event. It was calculated separately in each view and then summed in quadrature.

**emult**, the mean number of hit strips per hit plane associated to the candidate electron.

**plgapmin**, the lowest of  $plgapx$  and  $plgapy$ , provided they were not zero.  $plgapx$  and  $plgapy$  are the last hit gap before the first gap encountered along the track.

## 2.4 The overall background rejection strategy

The intrinsic  $\nu_e$  in the beam provides the most important background. Since these events are identical to the signal events but of predominantly higher energy, the only cuts that will eliminate them are cuts on the total number of hits in the event,  $tothit$ , and on the number of hits associated to the candidate electron,  $ensumht$ .

The other important source of background are  $\nu_\mu$ NC events in which a photon from a  $pizero$  converts close to the vertex thus simulating an electron. The direction of the candidate electron,  $ang$ , the fraction of the total energy of the event assigned to the electron,  $why$ , the closeness of the starting point of the track to the vertex,  $plgapmin$  and the net transverse momentum of the event,  $peet$ , can be used to reject this background.

Finally  $\nu_\mu$ CC events are also a source of background. In some cases a low energy muon can simulate an electron. Since, unlike muons, electrons shower, this background can be reduced with a cut on the multiplicity,  $emult$ . Note that, in the far detector, the  $\nu_\mu$ CC are greatly suppressed by  $\nu_\mu \rightarrow \nu_\tau$  oscillations.

The strategy was to reduce the  $\nu_\mu$ NC background to a level below that of the intrinsic  $\nu_e$  in the beam, while keeping the signal  $\nu_e$ CC efficiency as high as possible.

This was done in two steps: loose cuts followed by the use of likelihood functions to distinguish between signal  $\nu_e$ CC and background  $\nu_\mu$ NC events. The purpose of the loose cuts was twofold. Some of them were used to reject  $\nu_\mu$ CC and beam  $\nu_e$ CC events. In addition they all served in defining a definite range of variables for the likelihood functions used in the second step.

For each of the configurations, half of the event files available were used to study the background, define the loose cuts, generate the probability density functions used in the likelihood functions and decide on the cut on this likelihood that maximized the sensitivity of the experiment. The cuts and likelihood functions were then applied to the second half of the files, thus obtaining an

unbiased measure of the signal efficiency, the  $\nu_\mu$ NC,  $\nu_\mu$ CC and beam  $\nu_e$  backgrounds and of the sensitivity.

### 2.4.1 The loose cuts

In the following the readout strip width was taken to be 3cm.

Clearly the value of some of the above variables depended on the sampling frequency. Therefore the following cuts were configuration dependent:

#### **ensumht**

The range of ensumht for accepted events is given in the second column of Table 2.1. For events with **why** > **0.95** a tighter cut was applied: ensumht had to be larger than the value given in the third column of the table.

Table 2.1: Cut values for ensumht

Configuration	Cut range	why >0.95 events
6CM	$35 < \text{ensumht} < 180$	60
12CM	$24 < \text{ensumht} < 100$	40
24CM	$12 < \text{ensumht} < 50$	20
XORY	$12 < \text{ensumht} < 50$	20

#### **tothit**

This is equivalent to a total energy cut.

Table 2.2: Cut values for tothit

Configuration	Cut range
6CM	$60 < \text{tothit} < 200$
12CM	$32 < \text{tothit} < 100$
24CM	$16 < \text{tothit} < 50$
XORY	$16 < \text{tothit} < 50$

The upper cut on this variable is tighter than necessary for NC rejection but is necessary for rejecting intrinsic  $\nu_e$ CC events which are mostly of higher energy than the signal  $\nu_e$ CC. This can be seen in Fig. 2.2.

#### **peet**

The cuts on this variable were 80,40,20 and 20 for the 6CM, 12CM, 24CM and XORY samples respectively.

The following cuts were the same for all configurations:

**1.3 < emult < 3.0** The lower cut is tighter than necessary for NC rejection but is necessary for rejecting muons in  $\nu_\mu$ CC events as is illustrated in Fig. 2.3 for the 12CM sample.

**ang < 2.0**

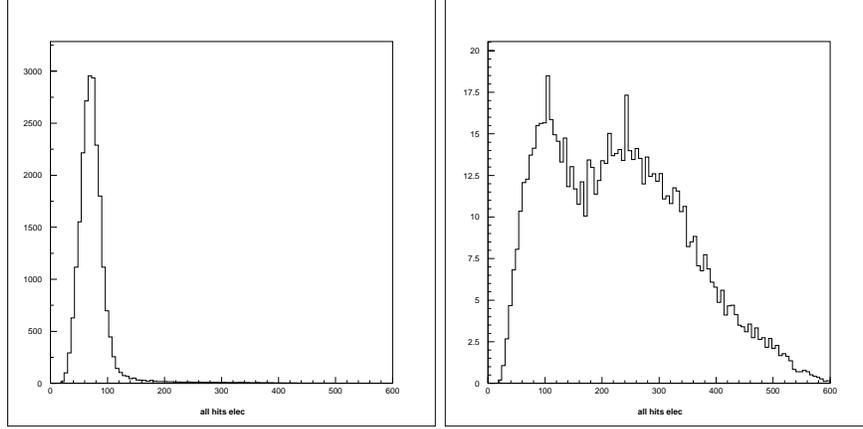


Figure 2.2: The distribution of total hits in the event for signal  $\nu_e$  (left plot) and intrinsic beam  $\nu_e$  (right plot)

**chimax < 100.0**  
**plgapmin  $\neq$  1.0**

### 2.4.2 The likelihood functions

Having applied these cuts, three two-dimensional probability density functions (pdf) were generated for signal events (PS) and for  $\nu_\mu$ NC events (PB). The pdf's used were:

- **ensumht vs why** referred to as **PS(sy)** and **PB(sy)**, Fig. 2.4.
- **ang vs tothit** referred to as **PS(at)** and **PB(at)**, Fig. 2.5.
- **chimax vs plgapmin** referred to as **PS(cp)** and **PB(cp)**, Fig. 2.6.

The procedure to generate each pdf was to generate a two-dimensional histogram of the relevant variables, smooth it and normalize it to unity. Note that different pdf's were calculated and used for each of the five configurations. The pdf functions were then used on the unbiased sample of events to obtain the quoted results. Given the values of the 6 variables, *ensumht*, *why*, *ang*, *tothit*, *chimax* and *plgapmin*, of an event, the probability that the event was of signal origin was computed as:

$$PS(sy) \times PS(at) \times PS(cp)$$

Similarly the probability of the event being of background origin was:

$$PB(sy) \times PB(at) \times PB(cp)$$

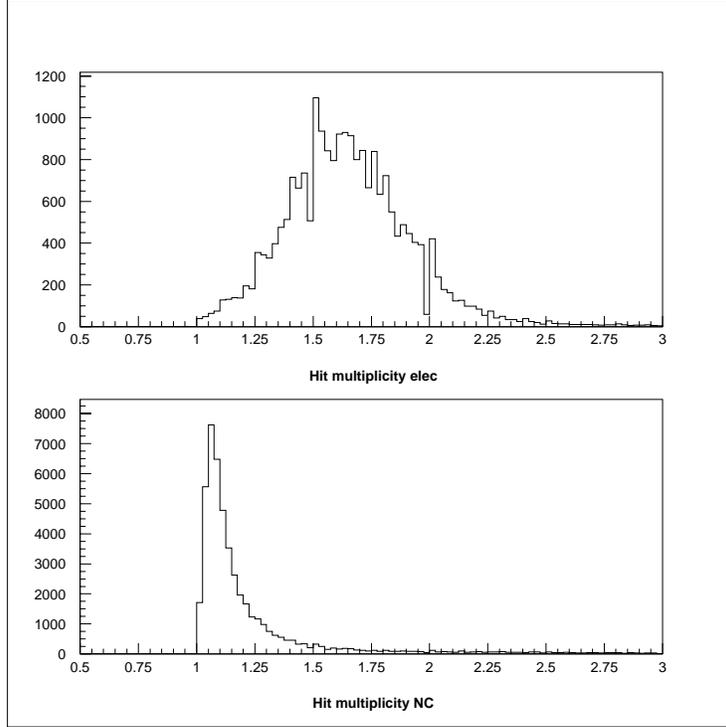


Figure 2.3: The mean number of hit strips per plane associated to the track for the 12CM configuration. Top plot for signal electrons and bottom plot for CC background

and the relative likelihood that the event was of signal or of background origin is given by:

$$L = \log\left(\frac{PS(\text{sy}) \times PS(\text{at}) \times PS(\text{cp})}{PB(\text{sy}) \times PB(\text{at}) \times PB(\text{cp})}\right)$$

An example of the signal and NC background likelihoods for the 12CM configuration is shown in Fig 2.7. In this case a cut on the likelihood of 3.25 was chosen (see next section).

## 2.5 Results

A Figure of Merit (FOM) was defined as:

$$\text{FOM} = \frac{\text{Number of signal events}}{\sqrt{\text{Total number of background events}}}$$

The FOM was calculated assuming:

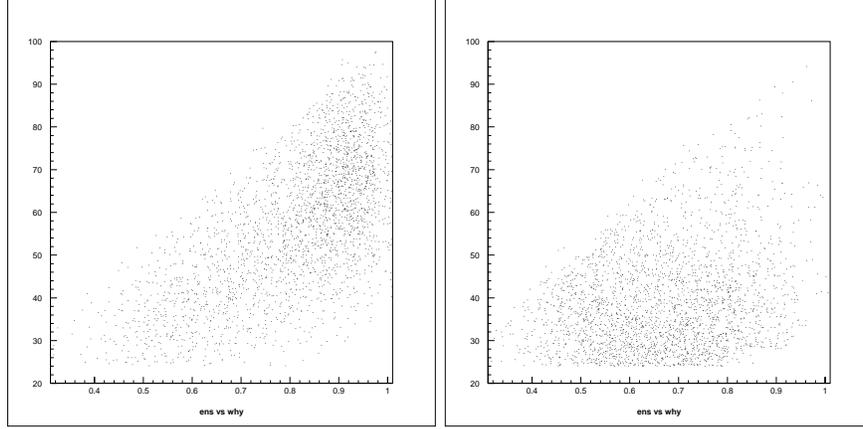


Figure 2.4: The ensumht vs why pdf two-dimensional distribution for signal (left plot) and NC background (right plot)

- $4.0 \times 10^{20}$  protons on target per year
- a 5 year run
- a 50 kiloton detector
- an 85% fiducial mass.

For each configuration, the numbers of signal and of background ( $\nu_\mu$ NC,  $\nu_\mu$ CC and beam  $\nu_e$ ) events, and, from these, the FOM were calculated as a function of likelihood cut. The FOM is a slowly varying function of the likelihood cut as is shown in the example of Fig. 2.8. However the background changes by a factor of three over this range of likelihood cut and the signal by a factor of two as can also be seen in Fig. 2.8. The cut that gave the maximum FOM was selected and used in the analysis of the unbiased event files

The signal efficiency and background rejection obtained are listed in Table 2.3 for the 12CM configuration as an example.

Table 2.3: Signal efficiency and background rejection for the 12CM configuration

Signal efficiency	Background Rejection		
	$\nu_\mu$ NC	$\nu_\mu$ CC	Beam $\nu_e$
0.35	$1.9 \times 10^{-3}$	$5.6 \times 10^{-4}$	$5.6 \times 10^{-2}$

With the detector and running scenario listed above the expected number of produced events are as follows:

$$\text{Events} = \text{Flux} \times \text{Years} \times \text{Mass} \times \text{Fiducial}$$

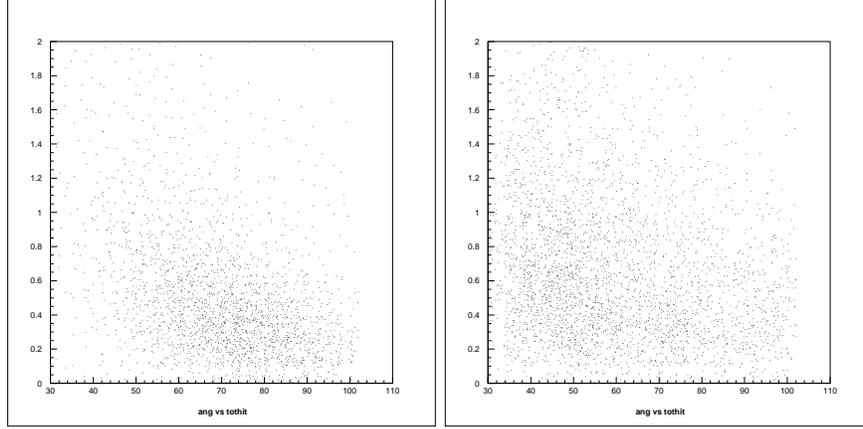


Figure 2.5: The ang vs tothit pdf two-dimensional distribution for signal(left plot) and NC background (right plot)

Number of  $\nu_\mu$ CC events before oscillations:

$$107.594 \times 5 \times 50 \times 0.85 = \mathbf{22863.7}$$

Number of intrinsic beam  $\nu_e$ CC events:

$$2.177 \times 5 \times 50 \times 0.85 = \mathbf{462.6}$$

Number of  $\nu_\mu \rightarrow \nu_e$  signal events:

$$\text{Events} = \nu_\mu \text{CC events} \times \text{oscillation prob.}$$

$$22863.7 \times 0.0293 = \mathbf{669.7}$$

The numbers of signal events and of background events from the three sources at the optimum FOM are shown in Table 2.4 for the four configurations, assuming the running conditions listed above.

Table 2.4: Numbers of signal and background events at the optimum FOM

Configuration	Signal	Background			Sum backg.	FOM
		$\nu_\mu$ NC	$\nu_\mu$ CC	Beam $\nu_e$		
6CM	208.9	7.6	2.1	24.3	34.0	35.8
12CM	232.2	12.9	5.3	25.8	44.0	35.0
24CM	217.7	20.6	8.7	27.3	56.6	28.9
XORY	213.6	13.6	4.9	24.3	42.8	32.6

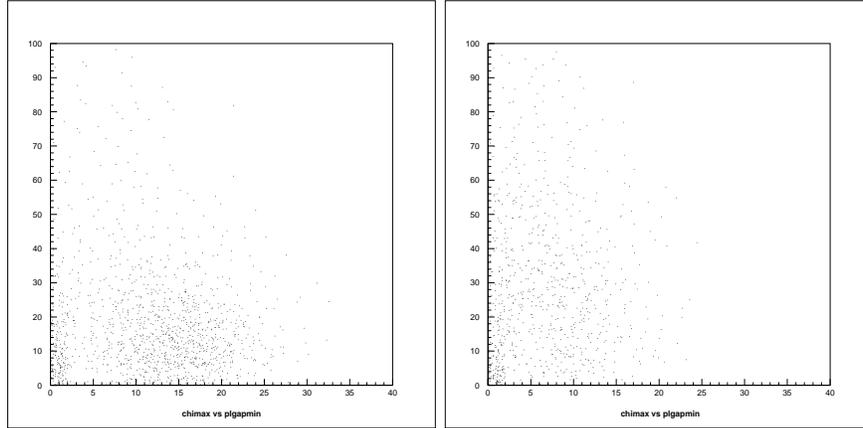


Figure 2.6: The chimax vs plgapmin pdf two-dimensional distribution for signal(left plot) and NC background (right plot)

## 2.6 The sensitivity as a function of absorber thickness

Three configurations were used in this analysis; 6CM,12CM and 24CM. The results are shown in Table 2.5.

Table 2.5: Dependence of the Figure of Merit on the Sampling Frequency

Configuration	Radiation length(%)	FOM
6CM	17.5	35.8
12CM	30	35.0
24CM	60	28.9

The uncertainty on these numbers is less than 1.0. Whereas reducing the absorber thickness by a factor of two does not improve the sensitivity significantly, doubling the thickness does worsen it by  $\sim 21\%$ .

## 2.7 The sensitivity as a function of active plane positions

Given a certain number of active readout planes, is it better to have both an x and a y plane together every D(cm) of absorber, Fig 2.9, or to alternate x and y every 0.5D(cm) of absorber, Fig 2.10?

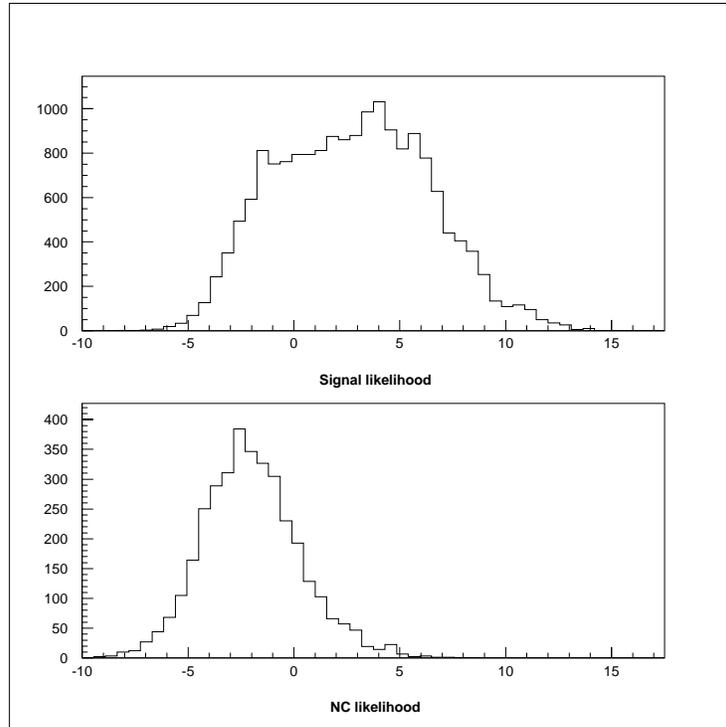


Figure 2.7: The signal and NC likelihoods for the 12CM configuration

Separating the x and y planes rather than lumping them together improves the FOM by **10%**. The reason for this improvement was traced to an improvement in the energy resolution of the detector when using a finer sampling, even though at each sampling only an x or a y are available. It goes from 17.2% in the 24CM configuration that samples every 0.6 rad. length to 15.0% in the XORY configuration that samples every 0.3 rad. length.

Table 2.6: Dependence of the Figure of Merit on the active plane position

Configuration	FOM
24CM	28.9
XORY	32.6

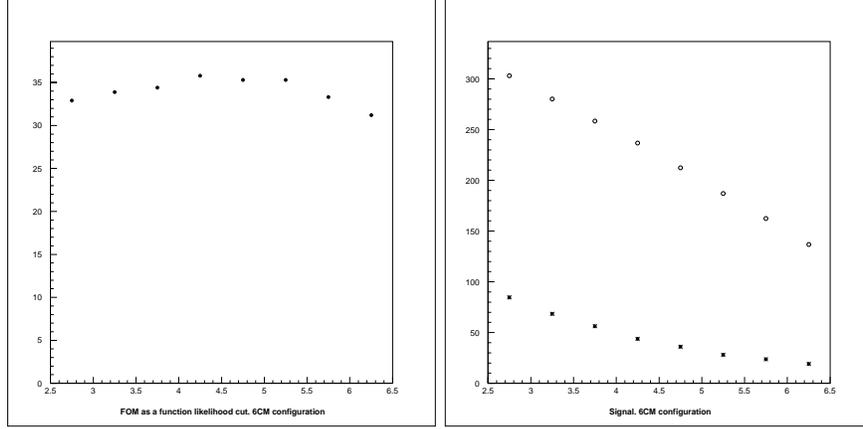


Figure 2.8: Left plot: The Figure of Merit as a function of likelihood cut. Right plot: The numbers of signal (open circles) and background (asterisk) events as a function of likelihood cut

## 2.8 Differences between $\nu_\mu \rightarrow \nu_e$ and $\bar{\nu}_\mu \rightarrow \bar{\nu}_e$

Since determining  $\theta_{13}$  and  $\delta_{CP}$  will require antineutrino running as well as neutrinos, the performance of the detector for antineutrinos was also investigated. Antineutrino events were generated, reconstructed and likelihoods were computed in the same way as described for neutrinos using the 30% radiation length geometry. This sample is referred to as 12BAR and is to be compared to the neutrino 12CM configuration.

As explained earlier the background arising from the  $\nu_\mu$  and  $\nu_e$  components of the antineutrino beam had to be taken into account. For completeness the background from the  $\bar{\nu}_\mu$  and  $\bar{\nu}_e$  components of the neutrino beam were also computed.

The signal efficiency and background rejection at the best FOM are summarized in Table 2.7.

Table 2.7: Comparison of the neutrino and antineutrino signal efficiencies and background rejections for the 12CM configuration

Configuration	Signal efficiency	Background Rejection		
		$\nu_\mu \text{ NC}$	$\nu_\mu \text{ CC}$	Beam $\nu_e$
12CM	0.35	$1.9 \times 10^{-3}$	$5.6 \times 10^{-4}$	$5.6 \times 10^{-2}$
12BAR	0.50	$2.0 \times 10^{-3}$	$3.0 \times 10^{-4}$	$6.7 \times 10^{-2}$

The signal efficiency for a comparable level of major component background rejection is much better in antineutrino running. This is because of the hadronic

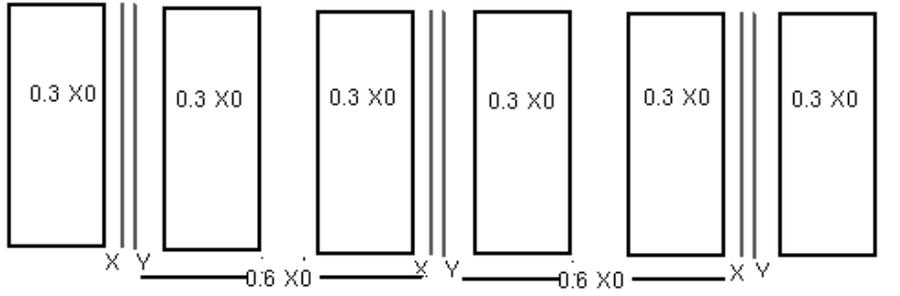


Figure 2.9: x and y plane together

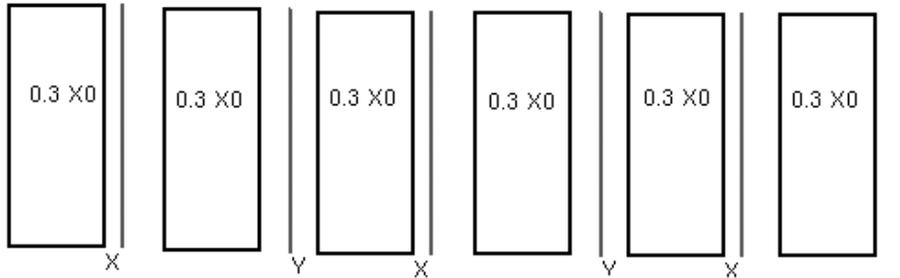


Figure 2.10: x or y plane alternating

energy in antineutrino events being lower, on average, than in neutrino events. The probability to simulate a signal electron of appreciable energy is therefore reduced in antineutrino events. However the background from the minor component ( $\nu_\mu$  and beam  $\nu_e$ ) is of comparable magnitude to the major component background.

The expected numbers of produced events for a 5 year antineutrino run are: **6880.3**  $\bar{\nu}_\mu CC$  events, **150.24** intrinsic beam  $\bar{\nu}_e CC$  events and **192.2** signal  $\bar{\nu}_e CC$  events.

Folding efficiencies and rejections results in the numbers of expected events shown in Table 2.8.

Thus, to have comparable significance in neutrino and antineutrino running, the antineutrino run will have to be  $(33.8/19.7)^2$  times as long as the neutrino run, i.e.  $\sim 3.0$  times longer.

Table 2.8: A comparison of the numbers of events expected in neutrino and antineutrino running

Conf.	Signal	Background						Sum backg.	FOM
		Major component			Minor component				
		$\nu_\mu$ NC	$\nu_\mu$ CC	$\nu_e$ Beam	$\nu_\mu$ NC	$\nu_\mu$ CC	$\nu_e$ Beam		
12CM	232.2	12.9	5.3	25.8	1.6	0.0	1.5	47.1	33.8
12BAR	96.1	4.6	0.8	10.1	4.3	0.6	3.3	23.7	19.7

## 2.9 Strip width studies

The sensitivity of the detector as a function of strip width was studied for the 12CM longitudinal segmentation. For each strip width studied the loose cuts and likelihoods were reoptimized. The results are shown in Table 2.9.

Table 2.9: Signal and background events and FOM as a function of strip width

Strip width	Signal	Background				Sum backg.	FOM
		$\nu_\mu$ NC	$\nu_\mu$ CC	Beam $\nu_e$	$\nu_e$		
2 <i>cm</i>	264.2	21.8	11.9	39.4	73.2	30.9	
3 <i>cm</i>	249.1	13.4	6.8	33.1	53.3	34.1	
4 <i>cm</i>	236.7	15.0	6.1	37.1	58.2	31.0	
5 <i>cm</i>	222.6	11.1	3.4	39.6	54.1	30.3	
6 <i>cm</i>	196.7	15.5	4.4	42.5	62.4	24.9	
7 <i>cm</i>	184.0	9.3	2.7	39.0	51.0	25.8	

## 2.10 Chamber efficiency studies

The effect of the chamber efficiency on the reconstruction of signal and background events was studied, [16], by eliminating hits at random according to the assumed chamber inefficiency in the 12CM sample with 3cm strips. Chamber inefficiency can be either due to spacer dead spaces or to an undeveloped streamer. The results are shown in Fig. 2.11 The efficiency for recognizing signal events drops with reduced chamber efficiency since the cuts are optimized for 100% chamber efficiency. However the more dramatic effect is the increase in the intrinsic beam  $\nu_e$ CC background with reduced efficiency. This is due to the fact that, because of their high energy and, hence, their large number of hits, a large fraction of these events just fail the upper cut on total hits. Reducing the efficiency moves these events into the accepted region. The background from  $\nu_\mu$ NC and  $\nu_\mu$ CC events is insensitive to the chamber efficiency.

For the measured efficiency of 93% these effects lead to an appreciable reduction in the FOM of about 8%. This was one of the reasons to double the number of RPC's at each gap, placing their spacers such that they would not overlap and thus increasing the combined efficiency for each active gap.

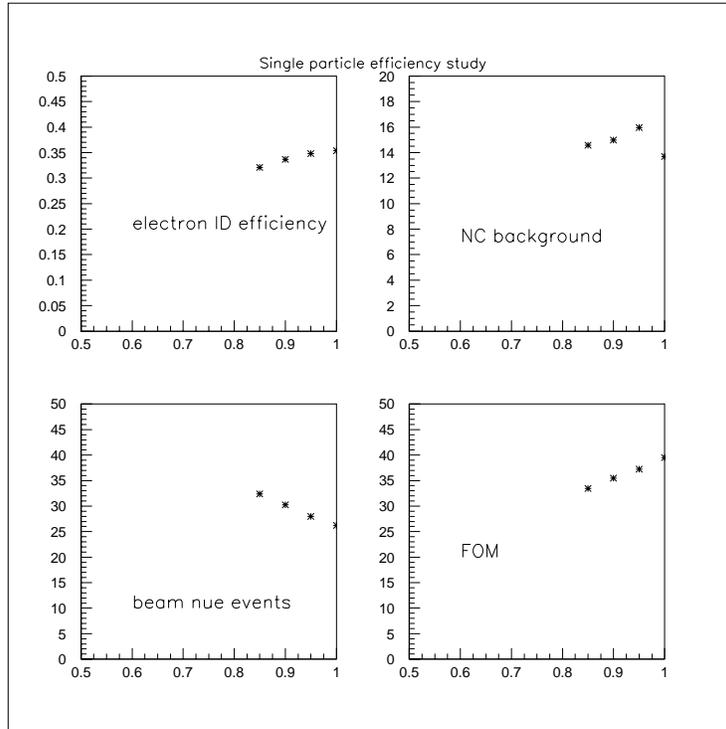


Figure 2.11: The signal  $\nu_e$ CC efficiency, the accepted number of signal and background events and the FOM as a function of the chamber efficiency

## 2.11 Cross Talk studies

The cross talk, is defined in this instance as the number of times a particle gives a signal in two strips, the one it traverses and an adjacent one. This cross talk may have an electronics contribution, independent of the actual position of the charged track within the strip, and a 'physical' contribution caused by the sharing of the produced signal for particles passing close to the boundary between two strips. We ignore this distinction and parameterize the cross talk in terms of a  $\chi$ , the cross-talk probability averaged over the strip. This probability, as well as the degradation of the FOM, will depend on the actual strip width. In this study we have assumed 3 cm wide strips. The amount of cross talk will

be reduced considerably for wider strips.

The effect of cross talk on the reconstruction of signal and background events was studied, [16], by adding the appropriate number of hits in strips adjacent to the ones hit in the 12CM sample with 3cm strips. The resulting numbers of reconstructed signal and background events are shown in Fig. 2.12 as a function of the amount of cross talk assumed. Because of their higher total number of hits, the number of beam  $\nu_e$ CC drops faster than the number of signal events; most of the accepted events have a total number of hits just below the upper cut on this variable and can therefore be eliminated when adding cross talk hits. The amount of  $\nu_\mu$ NC and  $\nu_\mu$ CC background increases with increasing cross talk. This is due to the fact that cross talk increases the number of hits per track, thus making charged pion and muons more shower-like. The FOM distribution indicates that the cross talk should be kept at a level smaller than 5%.

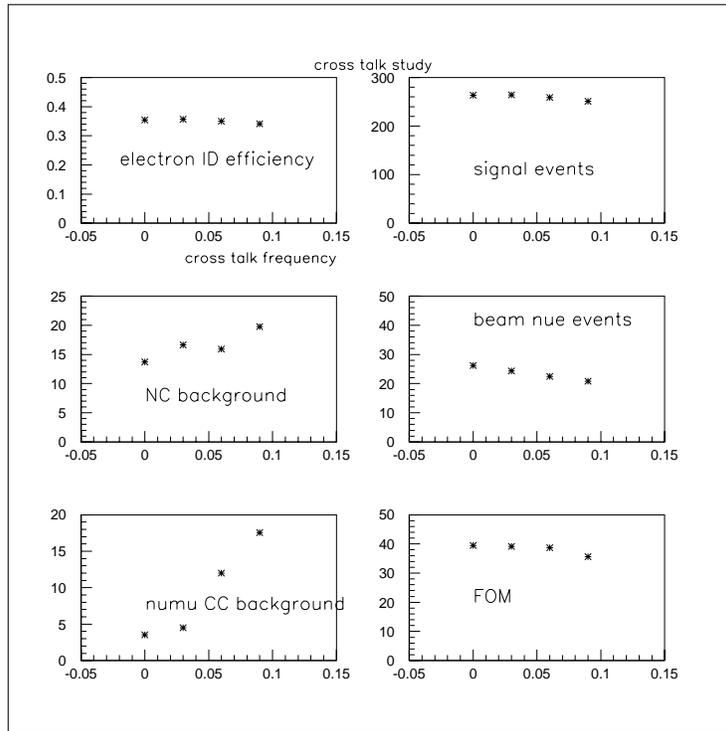


Figure 2.12: The signal  $\nu_e$ CC efficiency, the accepted number of signal and background events and the FOM as a function of the cross talk in RPC chambers

## 2.12 Dead space studies

The effect of dead spaces and cracks will require a proper analysis involving the full GEANT simulation of a realistic detector. We have developed an approximate treatment here, [16], assuming that the dead areas have similar material densities or that their relative contribution to the detector mass is rather small. Thus the shower development in the realistic detector is well approximated by the shower development in the ideal simulated detector. The effect of dead material and cracks on the reconstruction of signal and background events was studied by eliminating the appropriate number of hits in the 12CM sample with 3cm strips.

The dead material was assumed to be due to the vertical side plates of the modules. Their effect as a function of their thickness is shown in Fig. 2.13. Both the intrinsic beam  $\nu_e$ CC events and the  $\nu_\mu$  NC and CC events are not significantly affected by an increase in wall thickness. The signal is slightly reduced. Even for wall thicknesses of 5 cm ( a separation between modules of 10 cm) the decrease in the FOM is small.

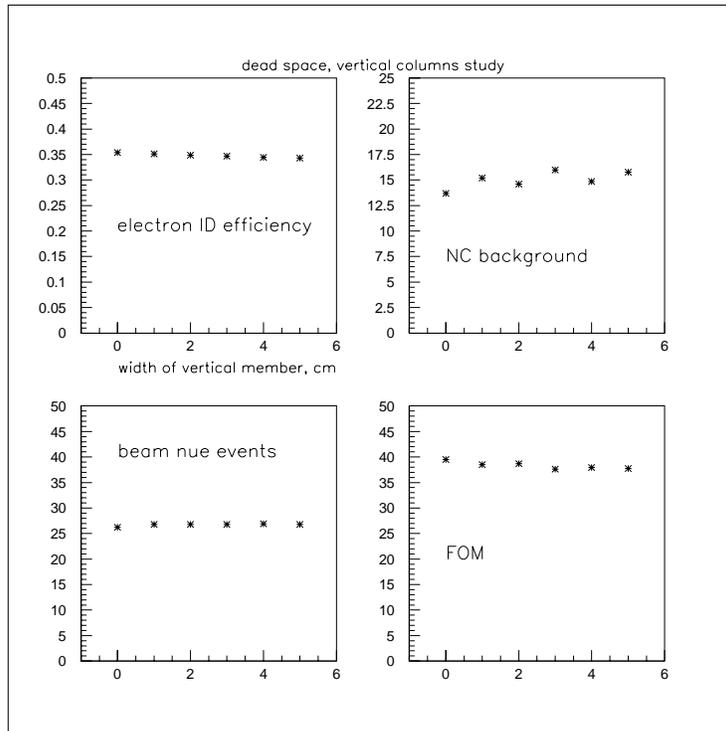


Figure 2.13: The signal  $\nu_e$ CC efficiency, the accepted number of signal and background events and the FOM as a function of dead space in the detector, in this case the thickness of the vertical side walls

## 2.13 Fiducial volume studies

The spatial extent of neutrino events in a low density detector is quite large. With detector density of the order of  $0.7 \text{ g/cm}^3$  the range of a  $0.5 \text{ GeV}$  particle is 3 meters or so, hence a significant fraction of the event energy can escape detection unless very stringent fiducial volume cuts are applied. Such cuts may lead to a significant loss of the useful mass of the detector. This effect was studied, [17], using the 12CM, 3cm strip width sample. The finite fiducial volume is simulated by ignoring all hits with transverse distance from the interaction point exceeding a  $\Delta x$  cut for the transverse fiducial studies or with longitudinal distance from the downstream edge of the detector exceeding a  $\Delta z$  cut for the longitudinal fiducial studies.

The signal efficiency and the number of background events in a 250kton-year exposure are shown in Fig. 2.14 as a function of  $\Delta x$ . The signal efficiency deteriorates when the event is produced near the edge of the detector. The intrinsic beam  $\nu_e$  events increase in importance near the edge of the detector as their usually high energy is underestimated because of the loss of hits and they therefore pass the upper cut on the energy. Similarly muons escaping the detector can also simulate electrons, increasing the  $\nu_\mu \text{ CC}$  background. The  $\nu_\mu \text{ NC}$  background is unchanged.

The signal efficiency and the number of background events are shown in Fig. 2.15 as a function of  $\Delta z$ . The signal detection efficiency starts to suffer when some of the energy of the signal events escapes detection. This happens at distances of the order of 4 m or less from the downstream end of the detector. For the same reason as in the transverse case, this leakage results in an increase of the beam  $\nu_e$  background. Neutral current background will be reduced as the visible energy distribution of the NC events is steeply falling. A 'resonant' increase of the  $\nu_\mu \text{ CC}$  background for the events occurring 4-6 m before the end of the detector is related to the total energy window used in the analysis to select signal events.

To study the optimization of the detector as a function of its transverse and longitudinal dimensions we have applied the following procedure:

- the total mass of a detector is kept constant at 50 kton.
- the detector length is calculated from the transverse dimension assuming an average density  $\rho = 0.7 \text{ g/cm}^3$ .
- curves fitted to the data shown in Figs. 2.14 and 2.15 are used as events density functions and the expected number of signal and background events is determined by integration over the detector volume.

The resulting FOM is shown in Fig. 2.16. As a function of the transverse dimension of the detector the FOM exhibits a very broad maximum corresponding to detectors in the range of  $15 \times 15 \text{ m}^2$  to  $25 \times 25 \text{ m}^2$ . Smaller detectors suffer from a deterioration of their performance due to the reduced signal and increased background around the edges of the detector. A drop of the FOM

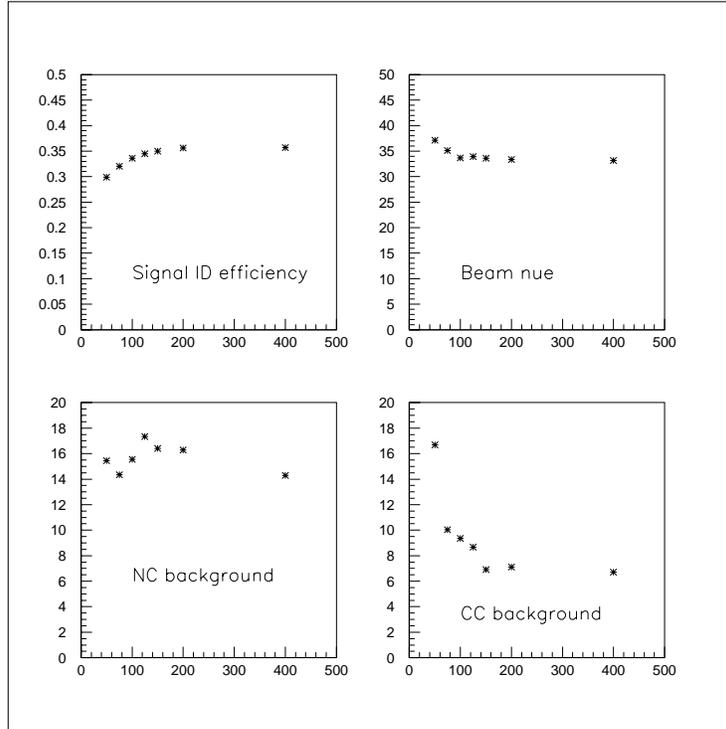


Figure 2.14: Top left: Efficiency for detection and identification of signal events ( $\nu_e$  interactions due to oscillations), as a function of the transverse distance, in cm, from the edge of the detector. Top right: Beam  $\nu_e$  background . Bottom left: Background due to  $\nu_\mu$ NC events, Bottom right: Background due to  $\nu_\mu$ CC events

for detectors of very large transverse size is due to the loss of the signal and increase of the background at the downstream end of the detector.

Comparison of these results with the FOM for a perfect detector indicates that in the optimized detector some 25% of the effective detector mass is lost because of edge effects.

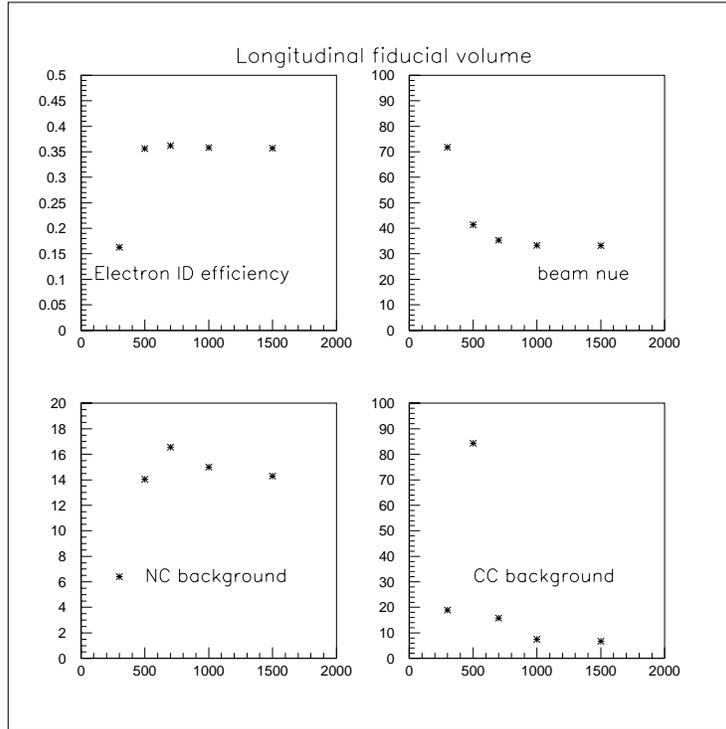


Figure 2.15: Top left: Efficiency for detection and identification of signal events ( $\nu_e$  interactions due to oscillations), as a function of the longitudinal distance, in cm, from the downstream end of the detector. Top right: Beam  $\nu_e$  background . Bottom left: Background due to  $\nu_\mu$ NC events, Bottom right: Background due to  $\nu_\mu$ CC events

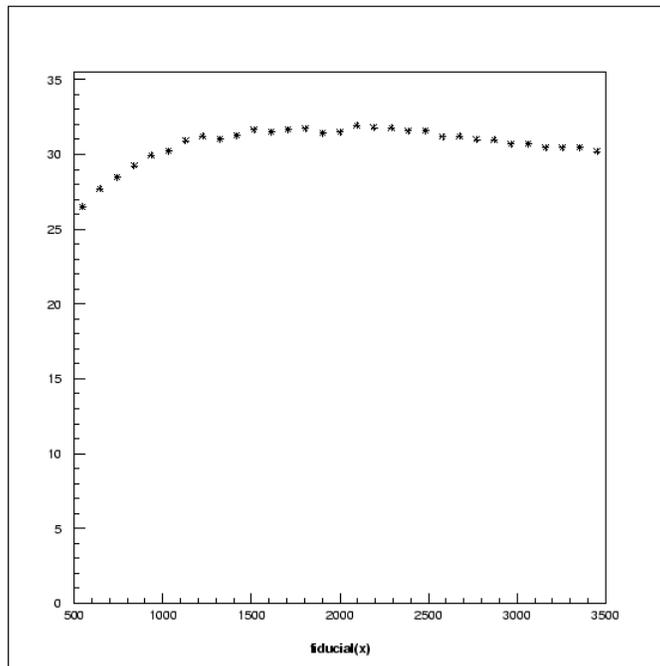


Figure 2.16: The FOM as a function of the transverse dimension, in cm, of the detector

# Bibliography

- [1] CERN-Hamburg-Amsterdam-Roma-Moscow experiment
- [2] Fermilab-IIT-Michigan-Moscow experiment
- [3] CHARM II experiment
- [4] the BELLE KLM detector group, Nuclear Instruments and Methods in Physics Research A 449 (2000) 112-124  
see also Nuclear Instruments and Methods in Physics Research A 456 (2001) 109-112
- [5] HARP experiment
- [6] P. O. Mazur, *Prepared for 3rd International Workshop on Resistive Plate Chambers and Related Detectors (RPC 95), Pavia, Italy, 11-12 Oct 1995*
- [7] ARGO experiment
- [8] N. Y. Agafonova *et al.* [MONOLITH Collaboration], LNGS-P26-2000.
- [9] Indian Neutrino Observatory
- [10] Jose Repond
- [11] Marcello Piccolo
- [12] C. Gustavino *et al.* A glass resistive plate chambers for large experiments, Nuclear Instruments and Methods in Physics Research A 457 (2001) 558-563
- [13] L. Camilleri, A. Para. The Reconstruction of  $\nu_\mu$  and  $\nu_e$  Monte Carlo events. Off-axis-NOTE-SIM-0011.
- [14] L. Camilleri, A. Para. A Study of an Off-axis Detector Performance as a function of sampling frequency. Off-axis-NOTE-SIM-0012.
- [15] Beam simulation program.

- [16] A. Para, Cross Talk, Cracks and Inefficiencies: how do they degrade the physics potential of a detector? Off-axis-NOTE-SIM-0017.
- [17] A. Para, Fiducial volume of the RPC detector. Off-axis-NOTE-SIM-0016.